Implementation of Optical Orthogonal Frequency Division Multiplexing through Polymer Optical Fibers

Catarina Faria Folgado

Thesis to obtain the Master of Science Degree in

Electrical and Computer Engineering

Supervisor(s): Professor Paulo Sérgio de Brito André

Professor Jair Adriano Lima Silva

Examination Committee

Chairperson: Professor José Eduardo Charters Ribeiro da Cunha Sanguino

Supervisor: Professor Paulo Sérgio de Brito André

Members of the Committee: Mário José Neves de Lima

November 2018

Declaration

I declare that this document is an original work of my own authorship and that it fulfills all the requirements of the Code of Conduct and Good Practices of the Universidade de Lisboa.

“The biggest obstacle to discovery is not ignorance: it is the illusion of knowledge.”

Daniel J. Boorstin

Acknowledgements

I would like to start by thanking my family for all the unconditional support. I would also like to thank my boyfriend Pedro and my friends, who not only supported me but gave me suggestions for this work.

I must also thank Professor Paulo André and Professor Jair Lima Silva for all the supervising, patience and guiding to overcome my obstacles in this work, and the Instituto de Telecomunicações (IT) for providing the laboratory and many equipment without which the experiment could not be performed.

Abstract

This work reports the transmission of an Orthogonal Frequency Division Multiplexing (OFDM) signal through a multimode step-index polymer optical fiber (SI-POF). This modulation scheme can be an interesting approach to increase the spectral efficiency of the system, since the channel presents a low bandwidth. Additionally, this technique also compensates the dispersion effects introduced by the fiber which are mainly dominated by intermodal dispersion. The transmissions performed in this work were based on direct modulation of LEDs and the non-coherent detection of the PIN photodiode. Bit rates of $26.6\ \mathrm{Mbit/s}$ with a link with 35 meters and a bandwidth of $5.7\ \mathrm{MHz}$ and bitrates of $19.3\ \mathrm{Mbit/s}$ with a link of 100 meters and a bandwidth of $4\ \mathrm{MHz}$ are shown.

Keywords: OFDM, LED, SI-POF, Spectral Efficiency, Optical Communications.

Resumo

Este trabalho tem como objetivo apresentar a transmissão de um sinal Orthogonal Frequency Division Multiplexing (OFDM) em fibras de plástico multimodo com step-index (SI-POF). Este método de modulação representa uma abordagem interessante para o aumento da eficiência espectral do sistema em questão, uma vez que o canal de transmissão apresenta uma baixa largura de banda. Adicionalmente, esta técnica permite compensar os efeitos dispersivos introduzidos pela fibra, que são maioritariamente dominados pela dispersão intermodal. As transmissões realizadas neste trabalho foram baseadas em modulação direta dos LEDs e na deteção não-coerente do foto-díodo do tipo PIN. Taxas de transmissão de $26{,}6\ \mathrm{Mbit/s}$ para uma ligação de 35 metros com uma largura de banda de $5.7\ \mathrm{MHz}$ e taxas de transmissão de $19{,}3\ \mathrm{Mbit/s}$ para uma ligação de 100 metros com uma largura de banda de $4\ \mathrm{MHz}$ são demonstradas.

Palavras-chave: OFDM, LED, SI-POF, Eficiência Espectral, Comunicações Óticas.

Table of Contents

List of figures

List of Tables

List of Acronyms

ACO-OFDM	Asymmetrically Clipped Optical OFDM
ADC	Analog to Digital Converter
ADO-OFDM	Asymmetrically Clipped DC biased Optical OFDM
ASK	Amplitude-Shift Keying
BER	Bit Error Rate
DAB	Digital Audio Broadcasting
DAC	Digital to Analog Converter
DC	Direct Current
DCO-OFDM	DC Biased Optical OFDM
DFT	Discrete Fourier Transform
DSP	Digital Signal Processing
FDM	Frequency-Division Multiplexing
FEC	Forward Error Correction
FFT	Fast Fourier Transform
FTTH	Fiber-To-The-Home
GOF	Glass Optical Fiber
ICI	Inter-Carrier Interference
IDFT	Inverse Discrete Fourier Transform
IFFT	Inverse Fast Fourier Transform
IM/DD	Intensity Modulation/Direct Detection
ISI	Inter-Symbol Interference
LAN	Local Area Network
LED	Light Emitting Diode
MCM	Multicarrier Modulation

MIMO	Multiple-Input and Multiple-Output
OFDM	Orthogonal Frequency-Division Multiplexing
OWC	Optical Wireless Communication
PAPR	Peak-to-Average Power Ratio
PMMA	Polymethyl Methacrylate
POF	Polymer Optical Fiber
PSK	Phase-Shift Keying
QAM	Quadrature Amplitude Modulation
QPSK	Quadrature Phase-Shift Keying
SEE-OFDM	Spectral and Energy Efficient
SER	Symbol Error Rate
SFO-OFDM	Spectrally Factorized Optical OFDM
SI-POF	Step-Index Plastic Optical Fiber
SNR	Signal to Noise Ratio
VLC	Visible Light Communication

1. Introduction

1.1. Motivation

Globally, the average number of devices and connections per capita will grow from 2.3 in 2016 to 3.5 by 2021 [1]. Figure 1.1 shows the trends of global Internet traffic in wired and wireless systems.

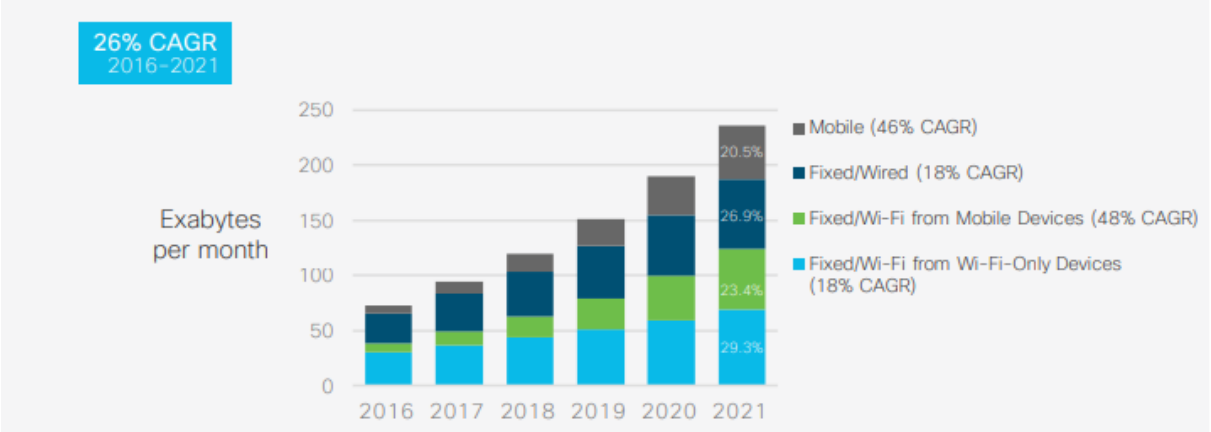

Figure 1.1 - Global Internet traffic, wired and wireless [1].

Figure 1.1 shows a 26 percent of compound annual growth rate (CAGR), from 2016 to 2021. By that time, wired devices will account for 27 percent of Internet traffic, and Wi-Fi and mobile devices will account for 73 percent of Internet traffic. In 2016, wired devices accounted for less than half of Internet traffic, at 38 percent. With this increase of devices per capita and global internet traffic it emerges the need of higher data rates, and with the consequently technology evolution associated with the glass optical fibers (GOF) in long distances, it emerged the need of technologies which could develop the same role over short distances [2], such as indoor and intra-vehicular networks. The polymer optical fiber (POF) technologies remained unused since its development in 1968, and only recently have been found application as a high-capacity transmission medium, due to the improvements in their transparency and bandwidth [3], and their price reduction in transmission and reception equipment. The outstanding obstacles to overcome in POFs are still their attenuation and dispersion values, which limits the bit rates and the connection lengths. With the promise of improving the capacity and spectral efficiency of the POF systems, several modulation schemes such as Orthogonal Frequency Division Multiplexing (OFDM) can be interesting to overcome its limitations at a low cost.

OFDM allows the reduction of the channel dispersive effects through the parallel information transmission with a set of orthogonal subcarriers. The spectrum of the individual subcarriers mutually overlaps, allowing to have a higher occupation of the system available bandwidth, comparing to the classical Frequency Division Multiplexing (FDM) [4]. The insertion of a guard interval helps to eliminate the inter-symbol interference at the transmission and the cyclic prefix is essential for the synchronization

at the reception. OFDM presents the great advantage of permitting the substitution of N modulators and filters for the digital processing through the direct and inverse discrete Fourier transform fast computing algorithms.

The technique presented in this work shows some differences relating to the wireless OFDM, which is well known and dominates the wireless communication systems. The use of Hermitian Symmetry leads to the creation of a purely real signal, which is going to directly modulate the light emitting diode (LED) and is going to be transmitted through the polymer optical fiber, and at the reception a PIN photodiode is responsible for the non-coherent signal detection.

1.2. State of the Art

In developed countries, fiber-to-the-home (FTTH) services that connect homes with a GOF backbone are well established. However, intrabuilding networks with GOFs have not yet been well developed because of its high price and difficult installation. Figure 1.2 shows the difference between the GOF (on the left side) and POF (on the right side), and their general construction.

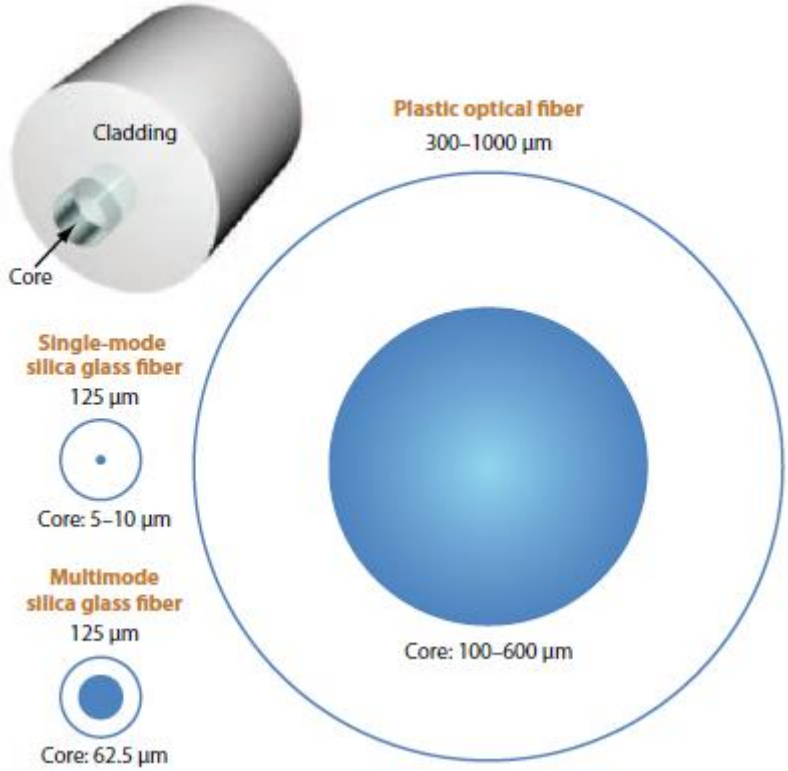

Figure 1.2 - Representation of the general construction of an optical fiber: single-mode GOF, multimode GOF and SI-POF [5].

The first POF was developed by DuPont in 1968, which was a multimode fiber with a step-index (SI) profile in the core region, however its attenuation was still about 1000 dB/km. During the eighties decade

it became possible to reduce losses nearly to the theoretical limit of approximately 125 dB/km at a wavelength of 650 nm, increasing the transparency of the fiber, and in 1975 the first commercialized (SI-POF) was introduced by *Mitsubishi Rayon*, named *Eska*, and subsequently other companies entered the market. The first POFs had high numerical apertures, translating into a large number of propagating modes, which has the great disadvantage of modal dispersion, leading to a lower bandwidth. The first POF with lower values of numerical aperture (NA) was presented again by *Mitsubishi Rayon* in 1995 [6]. The first single-mode POF was developed by Koike [7] in 1992. However, the attenuation coefficient was still very high compared to single-mode GOF and the ease of handling and low price were lost. In 2005 the first graded-index (GI) POF was produced in Korea by *Optimedia Co.,* as an approach to reducing modal dispersion. Figure 1.3 shows the difference in the refractive index profile between SI-POF and GI-POF.

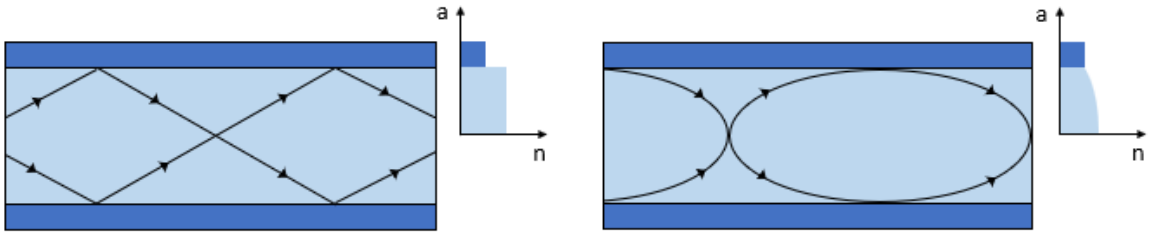

Figure 1.3 - Refractive index profile and ray path for a SI-POF (left) and GI-POF (right). a represents the distance between the central fiber axis and the cladding, and n represents the refractive index of the fiber.

Over the years, many studies have been conducted on Gigabit Ethernet over SI-POF and transmission rates exceeding 1 Gbit/s with the adoption of OFDM modulation have been achieved [8].

The first proposal of orthogonal frequencies for transmission appears in 1966 when Robert W. Chang published a paper [9] about his method for transmitting data simultaneously through a linear and band-limited channel without causing inter-symbol interference (ISI) and inter-carrier interference (ICI). Right after Chang, in 1967, Saltzberg performed an analysis [10] about Chang's paper and he concluded that "the strategy of designing an efficient parallel system should concentrate more on reducing crosstalk between adjacent channels than on perfecting the individual channels themselves, since the distortions due to crosstalk tend to dominate". Because of the development in digital signal processing (DSP), in 1971 Weinstein and Ebert [11] used the "fast" implementation of discrete Fourier transform (DFT), fast Fourier transform (FFT), to perform baseband modulation and demodulation. Since then there was the need to have banks of subcarrier oscillators, and this study introduced efficient processing, eliminating this problem. In 1980, Peled and Ruiz [12] considered that the OFDM formulation so far disregarded "any channel effects such as: phase jitter, amplitude modulation jitter, different types of noise, sampling jitter, and also differences in clock rates between the receiver and the transmitter", which caused ICI once the subcarriers were not perfectly orthogonal. They solved this orthogonality problem introducing the Cyclic Prefix (CP), which is a cyclic extension of the OFDM symbol, instead of using empty guard intervals. The use of a CP simulated a channel performing cyclic convolution ensuring orthogonality over

a time dispersive channel and eliminating ISI completely between subcarriers, as long as the CP remained longer than the impulse response of the channel. This introduced an energy loss proportional to the CP length, but it compensated to not have ICI. The inclusion of FFT and CP in OFDM systems made it very important in the telecommunications field.

Cimini, in 1985 [13], simulates the application of OFDM in mobile radio systems, using a technique for combating the effects of multipath propagation and cochannel interference. Digital audio broadcasting (DAB) was the first commercial application of OFDM and its development started in 1987 by Alard and Lassalle [14]. They considered the use of OFDM for radio broadcasting and concluded about the importance of combining the use of forward error correction (FEC) with OFDM, and because of this relation OFDM is often called coded OFDM (COFDM). The DAB standard was adopted in Europe in 1995.

In 1991, Chow and others [15] demonstrated the potential of OFDM as a modulation technique for high-bit-rate digital subscriber line (HDSL). A few years later emerges the development of digital video broadcasting (DVB), and in 1998 Reimers [16] published the development of DVB Project and its applications. In 2002 Ye Li and others [17] considered multiple antennas to form multiple-input and multiple-output (MIMO) channels to increase the capacity by a factor of the minimum number of transmit and receive antennas, to exploit ISI and enhance system capacity.

One of the major drawbacks of multicarrier transmission is the high peak-to-average power ratio (PAPR) of the transmit signal, since it enhances the non-linear effects of optical fibers. High PAPR also requires a high dynamic range of linear power amplifiers such as digital to analog converter (DAC) and analog to digital converter (ADC). There are several techniques to reduce it at the cost of loss in data rate, transmit signal power increase, bit error rate (BER) increase or computational complexity increase, and they should be chosen according to some systems requirements. There is an overview of this techniques written by Han and Lee [18].

OFDM exists in many wireless applications, such as the standard IEEE 802.11a used in wireless local area network (WLAN) [19] [20] [21], wireless metropolitan area networks (WMAN) [22] [23] [24], namely the standard IEEE802.16 which specifies fixed broadband wireless access techniques for point-to-point and point-to-multipoint links, asymmetric digital subscriber line (ADSL), digital subscriber line (DSL) modems [25], Wi-Fi [26], long-time evolution (LTE) (the fourth generation of mobile communications) [4], broadband power-line communication (BPLC) systems [27] and TV and radio broadcasting, as mentioned before. OFDM-based systems combined with MIMO techniques are being proposed as one of the technologies to be implemented for 5G cellular networks [28] [29].

The use of OFDM for optical communications emerged very recently, but there is already a great development in optical wireless communication (OWC) systems [30] [31] [32], single-mode optical fibers [33] [34] [35], multimode optical fibers [36] [37] [38], POFs [39] [40] [41], fiber-based optical access networks [42] [43] and outdoor free-space optics (FSO) [44].

Visible light communication (VLC) using light emitting diodes (LEDs) has been increasing attention recently due to its many advantages such as low power consumption, long lifetime, low cost and small

size [45]. The simplest and cost-effective way to realize VLC transmission is through intensity modulation/direct detection (IM/DD). The light from LEDs is not coherent, so IM/DD is generally used and can only be transmitted purely real and unipolar signals. In conventional OFDM, the transmitted signals are bipolar and complex, but bipolar signals cannot be transmitted in an IM/DD optical system because the intensity of light cannot be negative. A straightforward way to have a real OFDM signal, instead of complex, is using Hermitian symmetry before performing the inverse fast Fourier Transform (IFFT), and then the bipolar signal can be converted to unipolar by adding a direct current (DC) bias, as in DC biased optical OFDM (DCO-OFDM). In DCO-OFDM, a DC bias is added to the signal to make it positive. However, the required DC bias could be very large due to high PAPR of the signal, which would greatly reduce the power efficiency of VLC systems. Several modified schemes have been reported in the literature for spectral efficiency improvement and/or PAPR reduction, such as asymmetrically clipped optical OFDM (ACO-OFDM): the transmitted signal is made positive, by clipping the original bipolar OFDM signal at zero and transmitting only the positive. In ACO-OFDM only the odd subcarriers transmit data symbols, with the cost of having only half of the spectral efficiency, while in DCO-OFDM all the subcarriers carry data symbols. DCO-OFDM is less efficient than ACO-OFDM in terms of average optical power for constellations such as 4-QAM (QPSK), 16-QAM, 64-QAM and 256-QAM, but for larger constellations, such as 1024-QAM and 4096-QAM, DCO-OFDM is more efficient [46].

1.3. Objectives

Given OFDM's potential, in this work I propose to study the implementation of the OFDM through SI-POFs. The first objective is concerned with the modulation and demodulation of the OFDM signal because they are the key processes for an efficient data transmission, and the second objective is to accomplish the transmission using the techniques and parameters defined in the first objective.

1.4. Dissertation structure

Chapter 2 starts by introducing the fundamental concepts to follow the work described here: the concepts of the polymer optical fibers, the optical transmitters and receivers, the OFDM principles and some performance evaluation methods are introduced.

Chapter 3 presents the computational work developed for this experiment. A *Matlab* script is used to create a fiber model and simulate its response as transmission channel, with the parameters used in the experimental work described in the following chapter.

In Chapter 4 all the details of the implemented experimental setups can be found as well as some explanations about the methods and calculations adopted to implement the experiment.

Chapter 5 presents and analyses the results obtained in the various work stages. The transmissions performed are commented and analyzed, and some conclusions are done concerning the quality of the results as well as the main sources of error.

The last chapter summarizes all the conclusions together with the successes and errors that occurred. Some improvements suggestions to be implemented in the future are also done.

2. Theoretical Background

In this section OFDM and polymer optical fibers are studied in detail. Polymer optical fibers are introduced in subsection 2.1 and its main concepts are explained. In subsection 2.2 the transmitters and receivers of an optical system are presented, and the non-linearity of the LEDs is discussed. Subsection 2.3 covers key principles of OFDM and the main keys for implementing an OFDM system are presented. In subsection 2.4 it is explained the concept of the performance evaluation and which method is used in this work.

2.1. Polymer Optical Fibers

POFs are made of Polymethyl Methacrylate (PMMA), with a large core diameter (0.125 - 2.0 mm) and a high numerical aperture (NA 0.3 - 0.5). It has been used in low-bitrate and short-distance applications (less than 100 m), as it has a low bandwidth-length product (~40 MHz x 100 m for standard SI-POF NA 0.5) with high attenuation (150 dB/km for 650 nm wavelength).

An optical fiber is composed by two main regions: the core and the cladding. The core is the region where the optical signal is mostly propagated, and the role of the surrounding cladding is to confine the optical signal in the core region and, to make sure that an optical signal ray can be guided along the fiber, the refractive index of the core n_{core} has to be slightly higher than the refractive index of the cladding $n_{cladding}$. In a step-index profile fiber the refractive index is constant across the entire section of the core and cladding while the optical signal propagates in straight lines (along a zigzag path) in the core region, being completely reflected at the interface between the core and cladding. Graded-index profile fibers (GI-POF) are made up of a cladding with a constant refractive index and a core with a refractive index dependent on the radius.

The refractive index contrast is a parameter that measures the difference between the refractive index of the core and the cladding, and is expressed by

$$\Delta = \frac{n_{core}^2 - n_{cladding}^2}{2n_{core}^2} \tag{2.1}$$

When the optical signal enters the fiber there is a maximum incident ray angle, and the numerical aperture is defined as the sine of this angle, described in the following expression [47]:

$$A_N = \sin \alpha_{max} = n_{core}\sqrt{2\Delta} \tag{2.2}$$

2.1.1. Dispersion and attenuation in optical fibers

An optical signal is distorted when it travels along the fiber. This is mostly a consequence of dispersion, which is one of the most important problems in an optical fiber. The dispersion effect causes

a different delay to each of the optical signal's components of an impulse, so that, at the detector, these components are registered with different arrival times. There are two types of dispersion: chromatic and modal.

Chromatic dispersion describes the effect that signals at different wavelengths propagate at different speeds. Modal dispersion is the biggest cause of dispersion and the primary source of ISI in POFs. The information-carrying capacity of an optical fiber is determined by its impulse response. The impulse response and hence bandwidth are determined by the modal properties of the fiber: due to its large core, some of the optical signal rays may travel a direct route, whereas others travel higher distances as they bounce off the cladding. These alternate paths cause the different modes to arrive separately at the receiving point, and therefore the impulse response expands. Figure 2.1 shows, as an example, the fastest ($\alpha = 0$) and the slowest ($\alpha = \alpha_{max}$) ray. This becomes a serious constraint on transmission because pulses can overlap and interfere with each other, making it impossible to receive the original signal. This type of dispersion only occurs in multimode fibers, as this type of fiber has a large core diameter. In single mode fibers the core has a small diameter, limiting the number of propagating modes to a fundamental one and elimination modal dispersion. The fundamental mode occupies the central portion of the optical fiber and has an energy maximum at the axis of the optical fiber core.

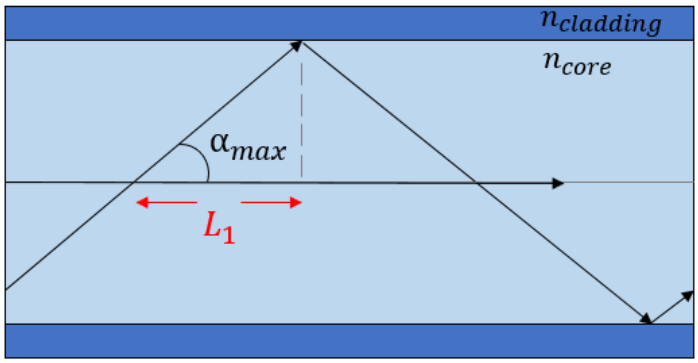

Figure 2.1 - Representation of modal dispersion in an optical fiber.

The expansion of the signal Δt is the time difference of the arrival of the slowest and fastest ray and is expressed as [2]

$$\Delta t = t_2 - t_1 = \frac{L_1 n_{core}}{c}\left(\frac{n_{core} - n_{cladding}}{n_{cladding}}\right) = \frac{L_1}{2c.n_{cladding}} A_N^2, \tag{2.3}$$

where A_N represents the numerical aperture of the fiber.

Distortion leads to a pulse broadening of the original signal and consequently the time gap between the bits becomes smaller and the pulses finally overlap, and the receiver cannot differentiate between the two. This leads to a reduction in the modulation amplitude of higher frequencies, making the fiber acting as a low-pass filter, and therefore it limits the transmission bandwidth:

$$B.L \approx \frac{0.44}{\Delta_t}.L_1, \tag{2.4}$$

where L is the length of the fiber. From the previous equation one can see that longer fibers have smaller bandwidths.

The change of the signal form by propagation along the fiber can be explained by signal theory and its impulse response:

$$s_1(t) = s_0(t) * h(t) + n(t), \tag{2.5}$$

where $s_0(t)$ and $s_1(t)$ are the signals at the beginning and at the end of the fiber, respectively, and $n(t)$ is the imposed Additive White Gaussian Noise (AWGN), mainly related with the receiver, as it is going to be detailed in subsection 2.2. The operator $*$ stands for a convolution. The impulse response $h(t)$ of the fiber is approximately Gaussian [48] and it can be expressed as

$$h(t) = \frac{\exp(-(t/\Delta t)^2)}{\sqrt{\pi}\Delta t} \tag{2.6}$$

Another important process to consider when the optical signal travels along an optical fiber is attenuation. The power of the optical signal decreases when propagating through the fiber with a length L and the power of the optical signal at the end of the fiber P_L can be described as:

$$P_L = P_0 e^{-\alpha'.L} \tag{2.7}$$

P_0 is the optical signal power at the beginning of the fiber with length L and α' is the value of the attenuation coefficient in km^{-1}. Attenuation α is usually expressed logarithmically in $\mathrm{dB/km}$.

$$\alpha = \frac{10}{L}\log\frac{P_0}{P_L} = 4.343\ \alpha' \tag{2.8}$$

Figure 2.2 shows the spectral attenuation curve of a standard SI-POF.

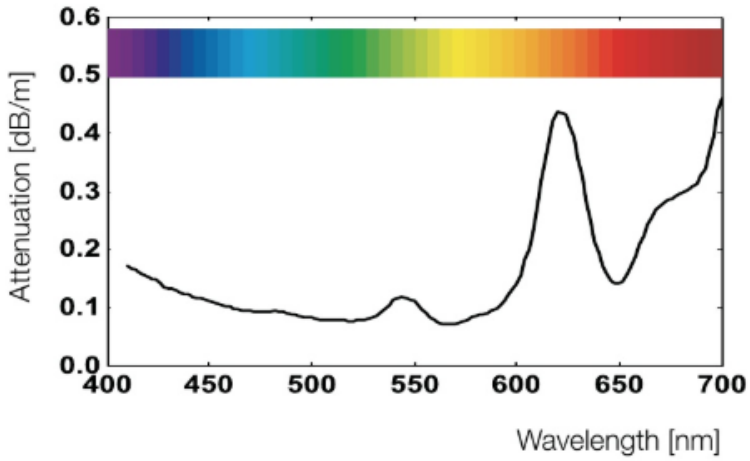

Figure 2.2 – Attenuation curve of a standard SI-POF [49].

Four different transmission windows can be identified observing the attenuation curve of a standard SI-POF: around 470, 530, 570 and 650 nm. Although there is a transmission window around the red optical signal (650 nm), the attenuation values around the blue and green optical signal (470 and 540 nm, respectively) are much lower than the attenuation around the red optical signal.

2.2. Optical transmitters and receivers

An optical system is essentially composed by three components: the transmitter, the optical transmission channel and the receiver. The transmitter is responsible for converting the electric signal into an optical one and sending it to the transmission channel which is, in this work, the polymer optical fiber. After the transmission channel has forwarded the signal to the receiver, the receiver converts it back into an electric signal. The goal is to make the received message as similar as possible to the transmitted one.

There are a large number of noise sources in optical systems. However, in short-range data communication, the components most responsible for the noise insertion are the transmitter and receiver components, such as light emitting diodes and photodiodes, respectively.

2.2.1. Light Emitting Diodes

The LEDs are the simplest form of a semiconductor device for electro-optical conversion and its simplicity, reliability and cost-effectiveness are very attractive for the use in optical short-range transmission. They are normally very low noise and stable sources and generate an optical signal through spontaneous emission, whose intensity is controlled by a unipolar electric current. To describe the effect of spontaneous emission, the light-emitting material is considered as a quantum mechanical system: p-type semiconductor containing positively charged carriers, called holes, is combined with n-type semiconductor material containing negatively charged carriers, called electrons, to create a diode.

When a current supply is connected to the diode in direct polarization, the negatively charged electrons are forced to move one direction, and the positive holes move in the opposite direction. A free electron and hole may recombine, generating a photon. This principle is described in Figure 2.3, where the system changes from a higher state (E_1) to a lower state of energy (E_0), emitting a photon of an energy of:

$$E_{photon} = E_1 - E_0 = hf = \frac{hc}{\lambda}, \tag{2.9}$$

where h is the Planck constant, f is the photon frequency, c is the speed of light and λ is the wavelength of the emitted photons.

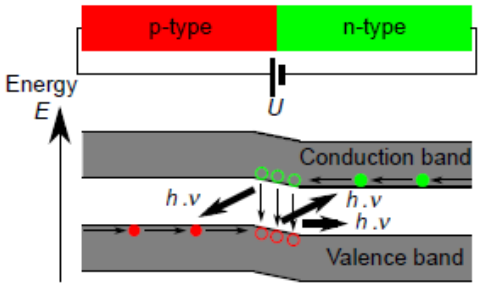

Figure 2.3 – Energy diagram of a p-n junction: principle of spontaneous emission [2].

The operation of modulation consists in transferring the data to be transmitted from the electrical to the optical domain. Two strategies can be used to perform this operation: the direct modulation and the external modulation. In the first strategy, the optical signal variates the intensity of the emitted optical signal. For example, in On-Off Keying (OOK) modulation, the transmitter emits the optical signal in each pulse emission, equivalent to the binary “1” and turns off in each emission equivalent to “0”. In the external modulation the intensity of the emitted signal remains constant and an external modulator is used to change the parameters of the signal, such as phase, amplitude, frequency, polarization and propagation direction, through electrical, magnetic or acoustical methods, in order to create a modulated signal. The major advantages of using direct modulation is its low cost and simplicity, since it does not require many equipment.

Like a diode the LEDs have a voltage threshold value known as “turn-on voltage”. For any value below that point it is considered the LED is not conducting current and for a voltage above that point its current (and the emitted optical power) increases exponentially with voltage. This relationship is shown in Figure 2.4, illustrating the application of direct modulation strategy. For this type of modulation, in order to control the distortion levels, the LED can operate around a bias point in a quasi-linear segment of its characteristics through DCO-OFDM.

The threshold voltage V_{th} value is related with the photons energy as described by:

$$V_{th} \geq \frac{E_{photon}}{q}, \tag{2.10}$$

where q is the electron charge constant.

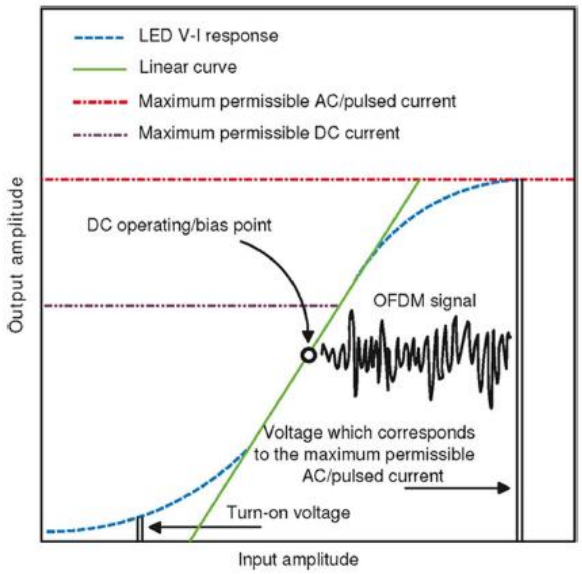

Figure 2.4 – Nonlinear LED transfer characteristic. Relationship between applied voltage and the emitted optical power [50], also is illustrated the application of direct modulation.

The LED current I_D can be described as a function on the applied voltage, as it can be observed in Figure 2.4.

$$I_D = I_S\left[e^{\frac{q(V-V_{th})}{K_B T}} - 1\right] \tag{2.11}$$

I_S is the reverse bias saturation current, T is the absolute temperature of the LED and K_B is the Boltzmann's constant. It can be observed, from equation (2.11), that the current is approximately zero until the applied voltage equals the turn-on voltage, and after that it increases exponentially with the applied voltage. However, as current increases, the LED characteristics become nonlinear, introducing distortions.

2.2.2. Photodiodes

The receiver is an important component for optical systems and besides the sensitivity, its response time is important for the transmission performance. Photodiodes convert the optical power P_{opt} into a photocurrent I_{ph}.The photocurrent generated by the incident photons represent the measured signal. In terms of efficiency, it is described by the external quantum power efficiency η_{ext}.

$$I_{ph} = P_{opt} \cdot \eta_{ext} \cdot \frac{\lambda}{1.24} \ \mu\text{m} \tag{2.12}$$

From the previous equation one can see that the smaller the optical signal wavelength the smaller is the photocurrent generated per watt of optical power. There is also another important parameter usually described in the datasheets for photodiodes, which is the responsivity $\mathcal{R}$, and it describes the emerging photo current per optical power in $\mathrm{A/W}$. Equation (2.12) can be rewritten in terms of responsivity:

$$I_{ph} = \mathcal{R} . P_{opt} \tag{2.13}$$

There are several structures of a photodiode, and the most important are the PIN photodiodes and the avalanche photodiodes (APD). The PIN photodiode is an improved extension of an ordinary p-n junction with an intrinsic layer in between. Figure 2.5 shows the structure of a PIN photodiode.

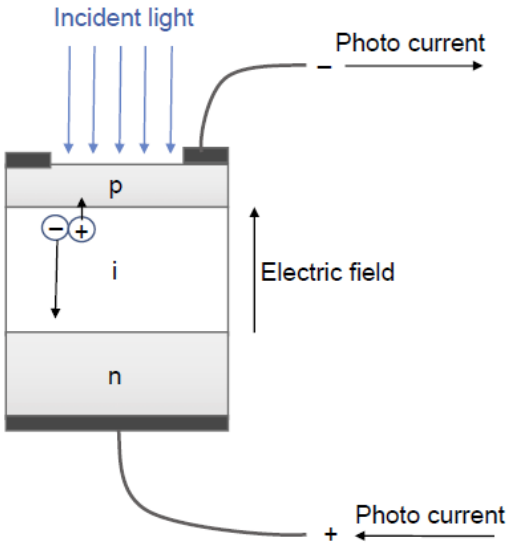

Figure 2.5 - General structure of a PIN photodiode and its basic principle of operation [51].

The incident optical signal enters the photodiode and it is absorbed in the semiconductor material. The energy of the absorbed photon is transferred to an electron in the valence band, which can be lifted into the conduction band. If there is an electrical field the free electron will be accelerated and drifts towards the positive electrode. Therefore, the total photo current rises or decreases depending if the intrinsic layer thickness rises or decreases, respectively.

An APD has an additional layer in the semiconductor structure that accelerates the generated electrons in a way that they gain enough energy to ionize other atoms and generate additional electrons that can be accelerated and ionize the same way. Therefore, the number of electrons generated can be much larger than the number of photons absorbed. Figure 2.6 shows the structure of an APD.

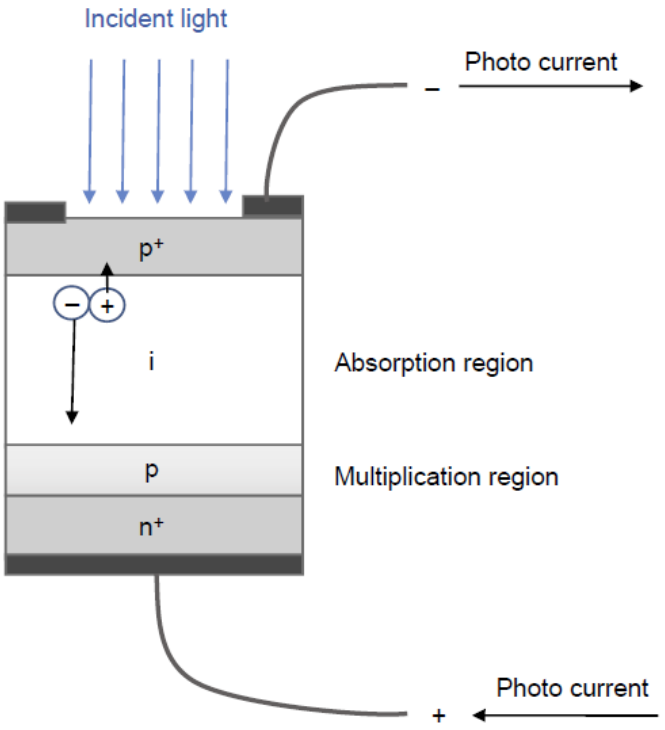

Figure 2.6 - Structure of an avalanche photodiode and its basic operation principle [51].

The PIN photodiode is the simplest and most used in POF systems. The advantage of it lies in its easy use because it only requires a bias voltage typically about 5 V to 15 V. The main advantage of the APD is that it has a greater level of sensitivity, about 10 dB more, compared to pin photodiode. However, because it requires a bias voltage that can reach 100 V to generate a higher electrical field and it has a large price, all commercial POF systems work with PIN photodiodes. In addition, the term avalanche refers to the output being non-linear and, as a result, APDs also produce a higher level of noise than pin photodiodes.

Every optical receiver can be described as a combination of a photodiode, an input resistor and an amplifier. Figure 2.7 shows the configuration of a typical POF receiver. The photocurrent is converted into a voltage at the input resistor and the greater the resistance is the higher the signal voltage, increasing the SNR. However, there is a fundamental limit: every photodiode has a junction capacitance which, together with the input resistor, forms a RC low pass filter, restricting the speed of the receiver. Consequently, the resistance can only be as high as the allowed by the photodiode capacitance and bandwidth, from which one can get the following relationship between the receiver's bandwidth B, its capacitance C and the input resistor R.

$$B = \frac{1}{2\pi RC} \tag{2.14}$$

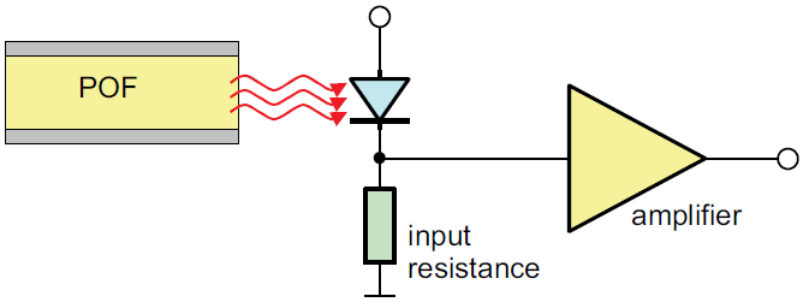

Figure 2.7 - Schematic of a POF receiver [51].

As with happens with LEDs, photodiodes also have a quasi-linear segment in its characteristics and, as the incident power increases, the forward current saturates, as it can be demonstrated in Figure 2.8.

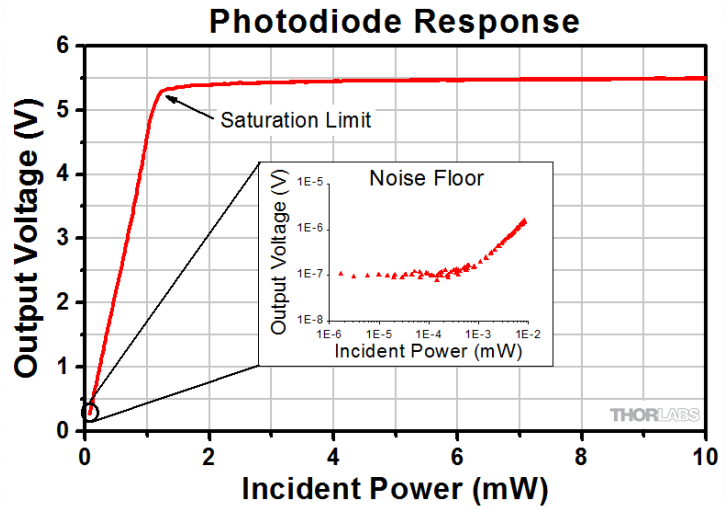

Figure 2.8 - Dynamic characteristic of a photodiode as function of the incident optical power [52].

When it occurs the saturation of the photodiode, its characteristic becomes non-linear and the detected signal cannot de demodulated.

2.3. OFDM Principles

Due to the amazing growth of the wired and wireless services and demands over the years, the need of transmitting high data rates at high bandwidth efficiency emerged. In conventional serial data systems, the several symbols are transmitted one by one, in sequence, at some specified rate. This is called a single-carrier system. The frequency spectrum of each data symbol can occupy the entire bandwidth, imposed by the dispersive channel. Time dispersion is a signal distortion manifested by the spreading of the modulation symbols in the time domain, also known as delay spread. This may also be expressed in the frequency domain: the higher the delay spread the lower the coherence bandwidth, and therefore the higher the channel frequency selectivity. For a very high data transmission, the

duration of the symbols is very short, and the time dispersion is generally much greater than the symbol rate, hence introducing the phenomenon called inter-symbol Interference (ISI) (because of the frequency-selective fading), and the received signals can add destructively resulting in signal fading and a significant reduction of the received SNR (Signal to Noise Ratio). This fading is very difficult to compensate because its characteristics are random and may not be easy to predict. For single-carrier systems, this situation is compensated with the use of equalization techniques at the receiver, but there are difficulties to implement a real-time equalizer with a low-cost and compact hardware [53].

Another approach is to divide the available channel bandwidth into N subchannels (with a different carrier for each subchannel) and to transmit the data simultaneously. Assuming that the available bandwidth is represented by B, the number of carriers is $N = B/\Delta f$, where Δf represents the width of each subcarrier. If Δf is small enough, the frequency response of the channel $C(f)$ is approximately constant across each subband and each subchannel is nearly ideal, as shown in Figure 2.9. This solution suggests a multicarrier modulation (MCM) and it provides transmission rates close to the channel capacity. The carrier period in the OFDM system is $T = NT_{symbol}$ (where T_{symbol} is the symbol period of the single-carrier system). Increasing the number of carriers N reduces de data rate of each individual carrier and therefore the carrier period T is much longer than the time duration of the channel time dispersion. Accordingly, ISI affects all frequencies in each signal equally and it can be estimated and compensated with simple equalization (reception) techniques [54] [55].

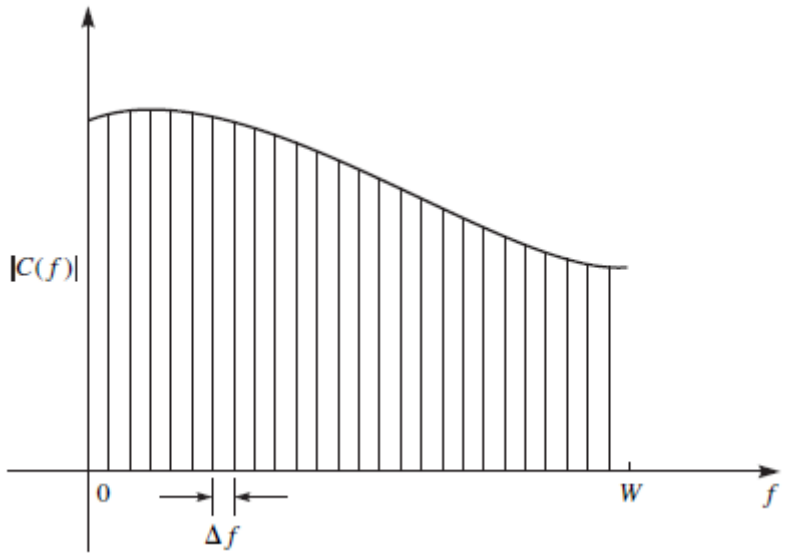

Figure 2.9 – Channel bandwidth W subdivision into narrowband subchannels of width Δf [55].

Unlike the classical frequency-division multiplexing (FDM) technique, in OFDM the subcarrier frequencies are chosen carefully so that the signals are mathematically orthogonal to one another over one symbol period. The spectra of individual subcarriers are allowed to overlap, although they can be demodulated without interference and the need for analog filtering to separate each subcarrier at the

receiver [56], thus increasing the spectral efficiency. The spectrum of the OFDM transmission is shown in Figure 2.10 and shows the bandwidth saving because of the use of OFDM.

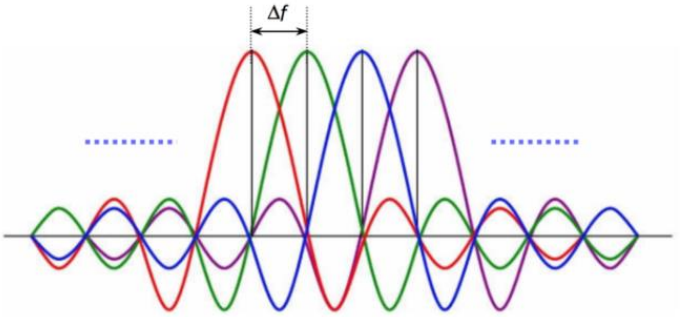

Figure 2.10 – OFDM transmission spectrum [57].

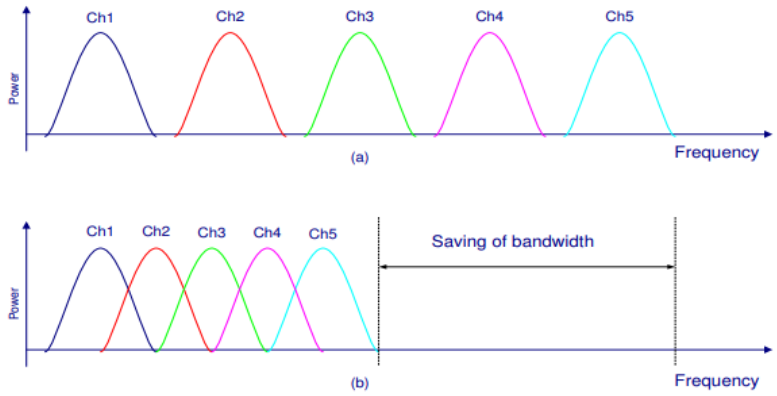

Figure 2.11 – Difference between conventional FDM and OFDM spectrum efficiencies [58].

The receiver may be viewed as a bank of demodulators translating each carrier to baseband and integrating over the symbol period to recover the data. As the subchannel spacing is selected to be an integral multiple of symbol periods, when integrating over the symbol period, the other carriers yield a zero contribution. This means that the subcarriers can be demodulated without the need to separate the received subcarriers, without interference.

The OFDM signal can be expressed in the time domain:

$$s(t) = \sum_{i} \left[\sum_{k=0}^{N-1} X_{i,k} e^{j2\pi f_k t} \right] g(t - iT) \tag{2.15}$$

The N data symbols $\{X_{i,k}\}_{k=0}^{N-1}$ are transmitted during the ith block and the set of complex sinusoids $\{e^{j2\pi f_k t}\}_{k=0}^{N-1}$ are referred to as the subcarriers. $g(t)$ is the pulse shape and is typically rectangular, as described in equation (2.16).

$$g(t) = \begin{cases} 1, & 0 \leq t \leq T, \\ 0, & \text{otherwise.} \end{cases} \tag{2.16}$$

The center frequency of the kth subcarrier can be expressed as

$$f_k = f_0 + k\Delta f, \qquad k = 0, 1, \ldots, N-1 \tag{2.17}$$

$\Delta f = 1/T$. Without loss of generality, one can let $f_0 = 0$. This way, equation (2.17) is simplified in equation (2.18).

$$f_k = \frac{k}{T} \tag{2.18}$$

Therefore, the orthogonality between subcarriers is proven and expressed mathematically as

$$\frac{1}{T}\int_0^T (e^{j2\pi f_k t})^* \left(e^{j2\pi f_j t}\right) dt = \frac{1}{T}\int_0^T e^{j2\pi (f_j - f_k)t}\, dt = \begin{cases} 1, & f_j = f_k \\ 0, & f_j \neq f_k \end{cases} \tag{2.19}$$

$(.)^*$ represents the complex conjugate operation.

As it is going to be demonstrated in section 2.3.2, OFDM systems are implemented using a combination of Fast Fourier Transform (FFT) and Inverse Fast Fourier Transform (IFFT) blocks that are mathematically equivalent to Discrete Fourier Transform and Inverse Discrete Fourier Transform, respectively, but more efficient to implement. An OFDM system maps the source symbols (with QAM, for instance) at the transmitter as though they are in the frequency domain. Hermitian Symmetry is applied in this work because an optical system was used, and the signal sent to the LED has to be real-valued. The IFFT is responsible for multiplexing an input signal onto a set of orthogonal carriers and it is applied to the sequence of the mapped symbols, converting information in the frequency domain to time domain. Any type of non-ideal transmission channel is going to cause the symbols to suffer dispersion, making the transmitted blocks to interfere with others. This is solved with a guard interval insertion in the output of the IFFT, called CP. After inserting the CP, the signal is submitted to a parallel-to-serial conversion and then it is converted to an analogue signal using a DAC. After that, the signal is ready to be transmitted in the channel. Figure 2.12 shows a block diagram of a simple OFDM system. When the OFDM signal reaches the receiver, its process is the same of the transmitter but backwardly: the signal is converted to digital using an ADC, the data are converted to parallel, the CPs are removed, and the signal is then demodulated using the FFT and the QAM demodulator, with the addition of a single-tap equalizer block next to the FFT and the removal of the Hermitian Symmetry next to the equalizer. The equalizer uses training symbols to estimate the channel characteristic, in order to compensate the distortion imposed by the transmission channel. Ideally, the output of the FFT would be the original symbols that were sent to the IFFT.

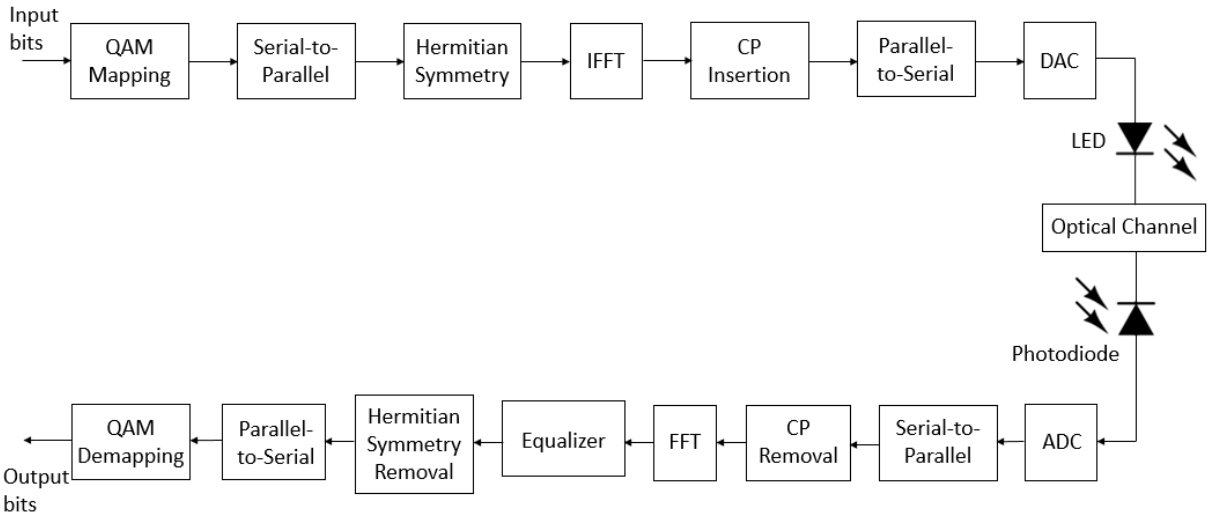

Figure 2.12 – Block diagram of an OFDM system.

All the blocks shown in the previous diagram are explained in the next subsections.

2.3.1. QAM Constellation

Each subcarrier of the OFDM signal is modulated using a modulation alphabet such as binary phase-shift keying (BPSK) modulation or even higher states modulation, such as 4-QAM, 8-QAM, 16-QAM, 32-QAM, 64-QAM, 128-QAM, 256-QAM, 512-QAM and 1024-QAM, with each symbol carrying multiple bits of information and therefore enabling high data rates, increasing spectral efficiency. The QAM is an amplitude and phase dependent modulation: it takes advantage of the orthogonality of a sine wave and a cosine wave, which are carrier waves. Each signal is multiplied either with a sine or cosine wave, and then those waves are summed, and the modulated signal is a mixture of amplitude-shift keying (ASK) and phase-shift keying (PSK) modulation. This technique is represented in a constellation diagram for different values of M-QAM, as shown in Figure 2.13.

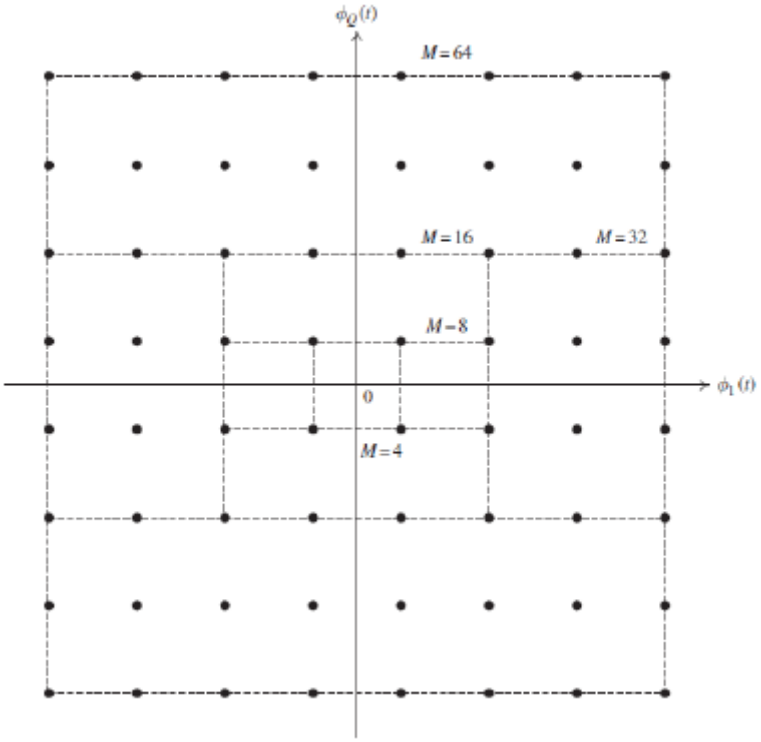

Figure 2.13 – Rectangular M-ary QAM constellations. $\emptyset_Q$ and $\emptyset_I$ are the axis of the carriers: the "quadrature" and "in-phase", respectively [59].

If each symbol is modulated with M-QAM, the signal on the kth subcarrier is given by equation (2.20).

$$u_k(t) = \sqrt{\frac{2}{T}} A_{kI} \cos(2\pi f_k t) - \sqrt{\frac{2}{T}} A_{kQ} \operatorname{sen}(2\pi f_k t) = \operatorname{Re}\left[\sqrt{\frac{2}{T}} A_k e^{j\emptyset_k} e^{j2\pi f_k t}\right] = \operatorname{Re}\left[\sqrt{\frac{2}{T}} X_k e^{j2\pi f_k t}\right] \tag{2.20}$$

$A_k = \sqrt{A_{kI}^2 + A_{kQ}^2}$, $\emptyset_k$ is given by equation (2.21) and $X_k = A_k e^{j\emptyset_k}$ is the signal point from the QAM constellation that is transmitted on the kth subcarrier. I represents the in-phase component and Q represents the quadrature component of the symbol.

$$\emptyset_k = \tan\left(\frac{A_{kQ}}{A_{kI}}\right) \tag{2.21}$$

When using QAM, the constellation points are normally arranged in a square grid with equal vertical and horizontal spacing and, as a result, the most common forms of QAM use a constellation with the number of points equal to 4, 16, 64, 256 and 1024. The constellation size depends on the number of bits per symbol: being b the number of bits, the constellation size is 2^b. By using higher order modulation

formats (more points on the constellation) it is possible to transmit more bits per symbol. However, since the range between 0 and 360 degrees will be divided into more regions, and those regions get smaller, the points are closer together and they are therefore more susceptible to noise and data errors, increasing the BER.

2.3.2. Mathematical Description of OFDM

For each subchannel it is associated a complex signal, which is defined as

$$s_c(t) = A_c(t)e^{j[2\pi f_c t + \emptyset_c(t)]} \tag{2.22}$$

$A_c(t)$ is the amplitude and $\emptyset_c(t)$ is the phase of the subcarrier, which vary for each symbol. For quadrature phase-shift keying (QPSK or 4-QAM), the amplitude is constant and the phase takes on one of four possible values per symbol. The transmitted bandpass signal is the real part of $s_c(t)$. In OFDM, the transmitted complex baseband signal for each subcarrier is

$$s(t) = \sum_{k=0}^{N-1} A_k(t)e^{j[2\pi f_k t + \emptyset_k(t)]} \tag{2.23}$$

f_k is the center frequency of the kth subcarrier and is represented by equation (2.18), and N is the number of information subcarriers. If the phase and the amplitude of the transmitted signal do not change over a symbol period, the amplitude and phase dependence on time can be disregarded and the equation (2.23) can be rewritten by equation (2.24).

$$s(t) = \sum_{k=0}^{N-1} A_k e^{j\left[\frac{2\pi k}{T}t + \emptyset_k\right]} \tag{2.24}$$

As mentioned before, $T = NT_s$, and since the subchannel spacing is selected to be an integral multiple of symbol periods, time can be expressed by $t = nT_s = \frac{nT}{N}$. So, in discrete time format each subcarrier is

$$s(nT_s) = \sum_{k=0}^{N-1} A_k e^{j\emptyset_k} e^{\frac{j2\pi kn}{N}} \tag{2.25}$$

Comparing equation (2.25) with the form of inverse discrete Fourier transform (IDFT), which is expressed in equation (2.26), one can note the similarity between the two.

$$x_N = \sum_{k=0}^{N-1} X_k e^{\frac{j2\pi kn}{N}} \tag{2.26}$$

It is obvious that the required time domain signal $s(nT_s)$ can be obtained through an IDFT of the symbol $A_k e^{j\emptyset_k}$, which can be taken from any QAM constellation, and OFDM subcarriers can be generated by the IFFT.

2.3.3. Hermitian Symmetry

Hermitian symmetry exploits a property of the discrete Fourier transform (DFT), specifically that the DFT of a real-valued signal has Hermitian symmetry. Therefore, to have a real output of the IFFT, an OFDM system with N subcarriers must hold to the conditions expressed in equation (2.27).

$$\begin{aligned} X_{N-k} &= X_k^* \\ X_{N/2} &= X_0 \end{aligned} \tag{2.27}$$

X_k is the complex value of the subcarrier with index $k \in [1,2,\dots,N/2-1]$. This can be achieved by mapping $N/2$ complex symbols to subcarriers of 0 to $N/2-1$ and assigning the respective conjugate value to the subcarriers of $N/2$ to $N-1$, at the cost of having only half subcarriers to carry data, obtaining the following relationship between the number of subcarriers carrying information N_{sc} and the number of subcarriers needed before the Hermitian Symmetry N_{HS}.

$$N_{sc} = \frac{N_{HS}}{2} - 1 \tag{2.28}$$

The IDFT is then

$$\begin{aligned} x[i] = \sum_{k=1}^{N-1} X_k e^{\frac{j2\pi ki}{N}} &= \sum_{k=1}^{N/2-1} X_{N/2-k} e^{\frac{j2\pi(N/2-k)i}{N}} + X_{N/2+k} e^{\frac{j2\pi(N/2+k)i}{N}} \\ &= \sum_{k=1}^{N/2-1} X_{N/2-k} e^{\frac{j2\pi(N/2-k)i}{N}} + X_{N/2-k}^* e^{\frac{j2\pi(N/2+k)i}{N}}, \end{aligned} \tag{2.29}$$

$i = 0,1,\dots,N-1$. But since

$$e^{j2\pi\left(\frac{N}{2}+k\right)i/N} = e^{j2\pi\left(\frac{N}{2}+k\right)i/N} e^{-j2\pi Ni/N} = e^{j2\pi\left(-\frac{N}{2}+k\right)i/N} = e^{-j2\pi\left(\frac{N}{2}-k\right)i/N}, \tag{2.30}$$

Equation (2.30) can be written as

$$x[i] = \sum_{k=1}^{N/2-1} X_{N/2-k} e^{\frac{j2\pi(N/2-k)i}{N}} + X_{N/2-k}^* e^{\frac{-j2\pi(N/2-k)i}{N}}, \tag{2.31}$$

$i = 0,1,\dots,N-1$. Using the identity $A + A^* = 2\mathrm{Re}\{A\}$,

$$x[i] = 2\mathrm{Re}\left\{\sum_{k=1}^{N/2-1} X_{N/2-k} e^{\frac{j2\pi(N/2-k)i}{N}}\right\} = 2\mathrm{Re}\left\{\sum_{k=1}^{N/2-1} X_k e^{\frac{j2\pi ki}{N}}\right\}, \qquad i = 0,1,\dots,N-1 \tag{2.32}$$

Since $\mathrm{Re}\{AB\} = \mathrm{Re}\{A\}\mathrm{Re}\{B\} - \mathrm{Im}\{A\}\mathrm{Im}\{B\}$,

$$x[i] = 2\sum_{k=1}^{N/2-1} \mathrm{Re}\{X_k\}\cos\left(\frac{2\pi ki}{N}\right) - \mathrm{Im}\{X_k\}\sin\left(\frac{2\pi ki}{N}\right), \qquad i = 0,1,\dots,N-1 \tag{2.33}$$

Therefore, $x[i]$ is real. Passing the sequence through a DAC yields the continuous-time real-valued OFDM signal:

$$x(t) = 2\sum_{k=1}^{N/2-1} \mathrm{Re}\{X_k\}\cos\left(\frac{2\pi kt}{T}\right) - \mathrm{Im}\{X_k\}\sin\left(\frac{2\pi kt}{T}\right) \tag{2.34}$$

2.3.4. Cyclic Prefix

In a dispersive optical channel, modal dispersion occurs, and different components of the signal arrive at different times, causing the distortion of its shape. Consequently, the subcarriers may interfere with one another, causing ICI, which may become a major problem resulting in ISI. To solve this problem, it is used a guard interval, called CP, and it is simply adding the copy of the last T_g seconds of the block at the beginning of each of them. If the duration of the CP is longer than the frequency response of the channel, the contribution of the previous block is entirely absorbed by the samples of the CP, that are discarded by the receptor. Note that if instead of using the CP it was used a “zero prefix”, which consists in a section of all zero samples transmitted in front of each block, this would destroy the periodicity of the subcarriers.

During the OFDM block interval, the waveform is given by equation (2.35).

$$s(t) = \sum_{k=0}^{N-1} X_k e^{j2\pi f_k t}, \qquad 0 \le t \le T \tag{2.35}$$

X_k are the data symbols and $e^{j2\pi f_k t}$ are the subcarriers. Derived from equation (2.18), the waveform of the block with the CP can be expressed as

$$s(t) = \sum_{k=0}^{N-1} X_k e^{j2\pi f_k (t+T)} = \sum_{k=0}^{N-1} X_k e^{j2\pi f_k t} e^{j2\pi k} = \sum_{k=0}^{N-1} X_k e^{j2\pi f_k t}, \qquad -T_g \le t < 0 \tag{2.36}$$

Thus, the OFDM signal having a guard interval with CP is simply

$$s(t) = \sum_{k=0}^{N-1} X_k e^{j2\pi f_k t}, \qquad -T_g \leq t \leq T \tag{2.37}$$

The price to pay because of the CP is the decrease of the transmission efficiency by a factor expressed in equation (2.38), which represents the ratio between useful and total transmission time.

$$\eta_g = \frac{T_u}{T_u + T_g} \tag{2.38}$$

T_u represents the useful symbol period and T_g represents the duration of the CP.

2.3.5. IFFT and FFT Algorithm

IFFT correlates the frequency domain input data with its basis functions, which are sinusoids at certain frequencies. Since the symbols are complex, the value of the symbol determines the amplitude and phase of the subcarrier sinusoid. The output of the IFFT is the sum of all N sinusoids. This way, the IFFT blocks provide a simple way to modulate information into N orthogonal subcarriers, since each frequency is chosen to create a set of orthogonal subcarriers. The output block with N samples construct the OFDM symbol.

The input of the IFFT is the complex vector $X = [X_0\ X_1 \dots X_{N-1}]^T$ and each element of the vector represents one QAM constellation point. The output of the IFFT is the complex vector $x = [x_0\ x_1 \dots x_{N-1}]^T$, and it is obtained by the expression in equation (2.39). As mentioned in section 2.3.3, the output of the IFFT is going to be a real vector instead of complex, because Hermitian symmetry is implied in the input.

$$x_n = \sum_{k=0}^{N-1} X_k e^{\frac{j2\pi kn}{N}}, \qquad 0 \leq n \leq N-1 \tag{2.39}$$

At the reception, as the basis functions of the FFT are not correlated, the correlation only sees the energy of the corresponding subcarrier. This separation of the signal energy is the reason why the spectra of each subcarrier can overlap without causing interference. At the FFT, the signal is correlated with the set of sinusoids to produce the original signal. The input of the FFT is the vector $y = [y_0\ y_1 \dots y_{N-1}]^T$ and it represents the samples in the time domain. The output is the vector $Y = [Y_0\ Y_1 \dots Y_{N-1}]^T$, and is

$$Y_k = \sum_{n=0}^{N-1} y_n e^{\frac{-j2\pi kn}{N}}, \qquad 0 \leq k \leq N-1 \tag{2.40}$$

To reduce the algorithm's complexity, it is necessary that the number of subcarriers is a power of two. If it is not the case, it can be extended with zeros, and this process is called zero padding. In order

to maintain the Hermitian symmetry, the zeros are inserted in the middle of the IFFT block. Therefore, the number of zero padding subcarriers can be defined as:

$$N_{ZP} = N_{IFFT} - N_{HS} \tag{2.41}$$

2.3.6. OFDM Equalizer

The equalizer is used at the receiver side to compensate the channel effects. The transmission channel causes signal distortion and, furthermore, it does not affect all the signal frequencies at the same way. If nothing is done, it would be impossible to obtain side the same data bits sent by the transmitter at the receiver.

Training symbols are commonly used to obtain the equalization function. This approach consists in sending, at the transmitter side, some training symbols, which are symbols which do not carry information. These symbols are only sent so that the receiver can know how the channel is affecting each different frequency. To make this possible, the receiver must know what the training symbols are and their position, so that when the received symbols arrive it can compare the training symbols received with the ones transmitted, knowing automatically how the transmission channel is affecting each one of the signal frequencies. By doing this, it is possible for the equalizer to respond to the channel by applying the inverse operation to each one of the signal frequencies, making it possible to recover the symbols sent by the transmitter. For a sequence of training symbols TS, the channel frequency response H_E is expressed as

$$H_E = \frac{s_{TS}}{S_{TS}}, \tag{2.42}$$

where s_{TS} is the received training sequence, and S_{TS} is the generated training sequence.

This transfer function has all the information about the transmission effects in the frequency domain and is enough to relate all the amplitude and phase differences of each subcarrier. To compensate these effects, the equalizer uses H_E^{-1} as the transfer function to mitigate all the distortions present in the transmission channel. The equalizer transfer function G_E is given by:

$$G_E = \frac{1}{H_E} = \frac{S_{TS}}{s_{TS}} \tag{2.43}$$

Although the training symbols decrease the system capacity in terms of information data, they are crucial for having a robust system. Note that, as the channel response changes in time, the training symbols must be sent periodically, in a period shorter than the channel coherence time (time in which the channel behavior does not change). The implementation of the equalizer device through numerical simulation does not make possible to recover the transmitted symbols with 100% precision. In fact, the received symbols after passing through the equalizer are not exactly equal to the transmitted ones. The

reason for this is the fact that the system presented is not linear and the equalizer only recovers the symbols in a perfect way for linear systems.

2.3.7. Spectral Efficiency

One of the major advantages of OFDM is its high spectral efficiency, because since OFDM uses overlapped orthogonal subcarriers, they occupy narrow bandwidth. To be able to study the spectral efficiency the concept of OFDM frame must be introduced. The frame is composed of N_{total} OFDM symbols and N_{sc} subcarriers. The total number of OFDM symbols are composed by the training symbols N_t, used for channel estimation, and data symbols N_{data}, responsible for carrying information data. The OFDM frame is represented in Figure 2.14.

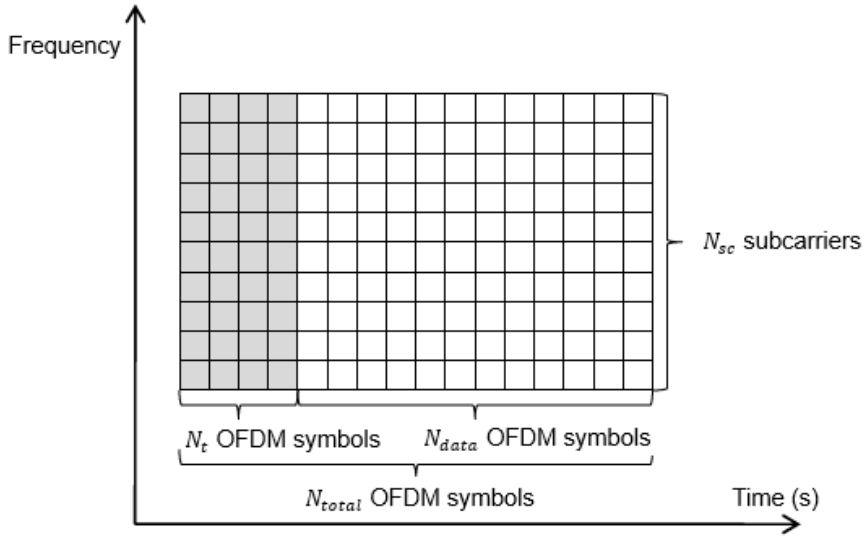

Figure 2.14 – OFDM frame representation.

In an ideal OFDM system without guard interval T_g and with all the subcarriers carrying data, the corresponding bit rate (bits per second) is defined by

$$R_b = \frac{N_{sc}}{T}\log_2 M \tag{2.44}$$

$\log_2 M$ represents the number of bits transmitted per subcarrier. With the insertion of the guard interval and the training symbols, the bit rate R_b is going to suffer a reduction:

$$R_b = \frac{N_{sc}}{T+T_g}\frac{N_{data}}{N_{total}}\log_2 M = \frac{N_{sc}}{T+T_g}\frac{N_{data}}{(N_t+N_{data})}\log_2 M \tag{2.45}$$

Considering Figure 2.10 and knowing that the frequency spacing between subcarriers is $1/T$, by using the first null to denote the boundary of each wavelength channel, the OFDM bandwidth can be defined as

$$B = \frac{2}{T + T_g} + \frac{N_{sc} - 1}{T} \tag{2.46}$$

The spectral efficiency is expressed in $\mathrm{b/s/Hz}$ and is given by

$$S = \frac{R_b}{B} = \frac{N_{sc} N_{data}}{2N_{total} + \frac{N_{total}(T + T_g)(N_{sc} - 1)}{T}} \log_2 M \tag{2.47}$$

In the case of an ideal OFDM system without guard interval, it can be considered that $N_{sc} \gg 1$ and $T_g = 0$, therefore the bandwidth can be simplified as

$$B = \frac{N_{sc}}{T} \tag{2.48}$$

For this system the spectral efficiency is then given by equation (2.49).

$$S = \frac{R_b}{B} = \frac{\frac{N_{sc}}{T}}{\frac{N_{sc}}{T}} \log_2 M = \log_2 M \tag{2.49}$$

Comparing equation (2.47) with equation (2.49), it can be concluded that there are two ways of improving spectral efficiency of an OFDM system: the first one is to use an high order modulation scheme, and the second one is to reduce the guard interval and the number of training symbols.

2.4. Performance Evaluation Metrics

When planning an optical fiber system, improving the received signal is always the main concern. In this section it is described the main figure of merit used for performance evaluation in the context of this work, the bit error ratio (BER).

To evaluate the quality of the transmission one can observe its BER, which is a function of SNR at the receiver. BER is a key parameter that is used in assessing systems that transmit digital data from one location to another. It quantifies the percentage of erroneous bits out of the total of transferred bits during a time interval. The definition of bit error rate can be translated into a simple formula:

$$\mathrm{BER} = \frac{\text{number of errors}}{\text{total number of bits sent}} \tag{2.50}$$

While the usual value of acceptable BER for an optical fiber system is of the magnitude of 10^{-9}, it is nowadays possible to meet the required quality standards with a BER of 3.8×10^{-3}. The reason for this

is the introduction of forward error correction (FEC) techniques, in which a percentage of the total bits is repeated to add redundancy to the signal. While a greater link capacity is needed, the signal will also be more resilient to bit errors. Therefore, to validate the results in this project a BER below the limit of 3.8×10^{-3} is required [60].

3. Computational Simulations

The purpose of this section is to present and describe all the computational aspects developed in this work obtained with *Matlab*, which is a software developed by *Mathworks* for numerical computing and programming language. In subsection 3.1 it is presented the description of the simulation used in this work, and subsection 3.2 is related to the simulation results obtained.

3.1. Simulation description

The transmission channel of this work can be represented as an additive white Gaussian noise (AWGN) channel. As mentioned in subsection 2.2 the most responsible component for this effect is the photodiode. The system also suffers from fading due to the dispersion of the signal in the POF, as mentioned in subsection 2.1.1. Therefore, there was created the system described in Figure 2.12, and for the transmission channel *Matlab* functions were used to insert the AWGN and it was created the fiber model to estimate the impulse response of the channel. The concept was to use equation (2.5) in order to perform a convolution between the signal and the frequency response of the equation (2.6), and then it was inserted the AWGN based on the SNR.

The energy per bit E_b $(\mathrm{Joules/bit})$ is related to the total signal power S and the transmission rate R_b:

$$E_b = \frac{S}{R_b} \tag{3.1}$$

Introducing the noise power N_o, the equation mentioned above can be written as the following:

$$\frac{E_b}{N_o} = \frac{S}{R_b N_o} \rightarrow SNR = \frac{E_b}{N_o} \times R_b \tag{3.2}$$

Therefore, the SNR in dB is expressed in equation (3.3).

$$SNR_{dB} = \frac{E_b}{N_{o\,dB}} + 10\log_{10} R_b \tag{3.3}$$

3.2. Fiber Model Simulation Results

The simulations were used to test the results obtained in the experimental part of this work. Therefore, the same parameters of section 4 were used, for 35 and 100 meters of fiber, detailed in Table 3. To simulate the 35 meters transmission 2700 samples were transmitted, with a simulation time of $10.92\ \mu s$ and 256 total subcarriers were used. With 2700 samples transmitted and 162 of them used for the equalizer, for 4-QAM, 16-QAM and 64-QAM, the total number of bits sent was 5076, 10152 and 15228, respectively. For the 100 meters transmission simulation 7650 samples were transmitted, with a simulation time of $30.81\ \mu s$ and 512 total subcarriers were used. With 7650 samples transmitted and

459 of them used for the equalizer, for 4-QAM, 16-QAM and 64-QAM, the total number of bits sent was 12690, 28764 and 43146, respectively.

Figure 3.1 shows the generated, which was obtained using equation (2.6), and estimated channel frequency response, which was obtained using equation (2.42), and they were created with *Matlab.* In Figure 3.2 it is presented the transmitted constellation diagram and transmitted signal in the time domain for 4-QAM, and from Figure 3.3 to Figure 3.5 there are presented the received constellation diagram of the received signal for 4-QAM, 16-QAM and 64-QAM, simulating the transmission over 35 meters of fiber, created with *Matlab*. Figure 3.6 shows the diagram of the obtained BER versus E_b/N_o for 4-QAM, 16-QAM and 64-QAM, for 35 meters of fiber.

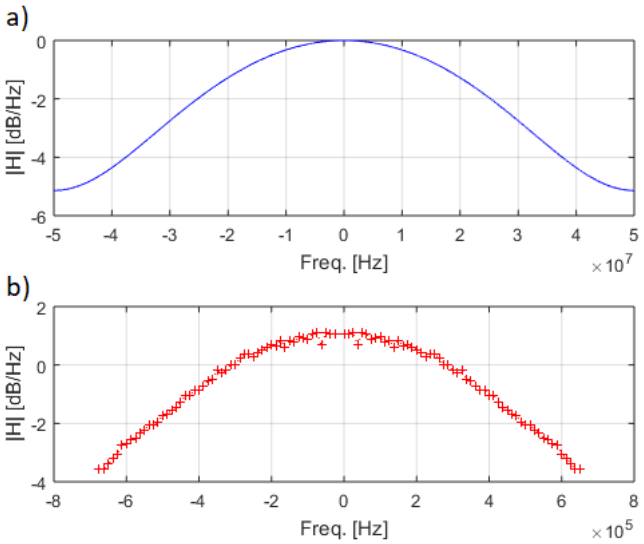

Figure 3.1 – a) The generated frequency response of the channel for 35 meters of fiber and for a E_b/N_o of 5 dB; b) The estimated frequency response for 35 meters of fiber and for a E_b/N_o of 5 dB.

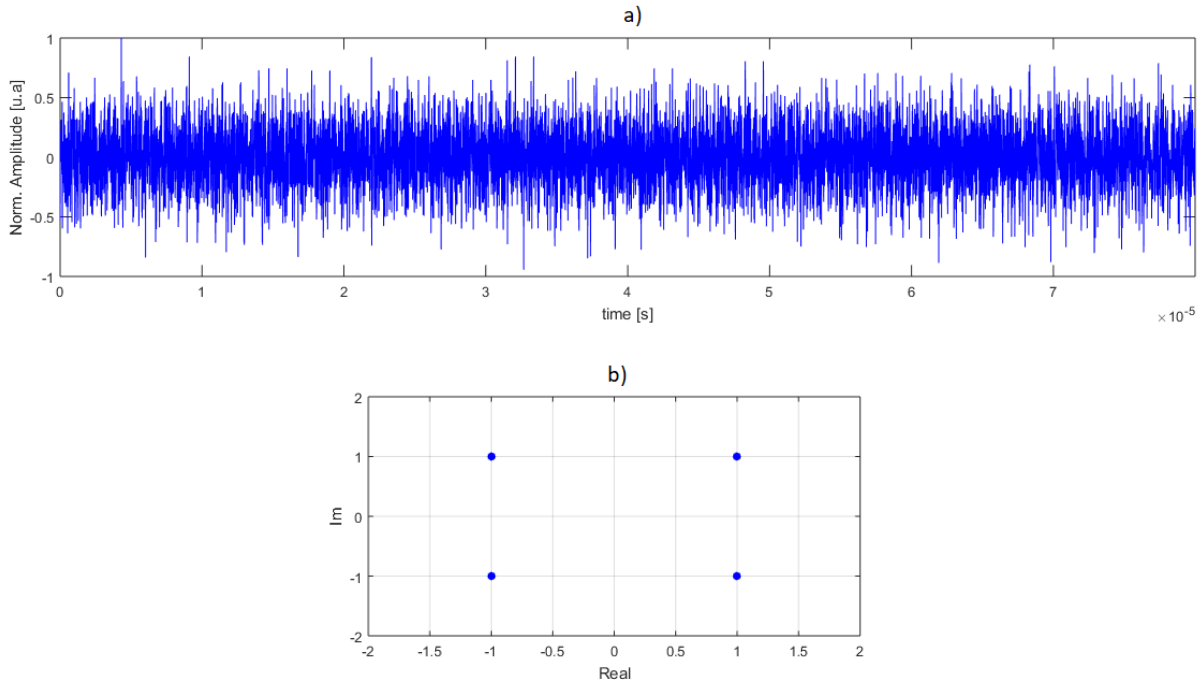

Figure 3.2 – a) Transmitted OFDM signal in the time domain for 35 meters of fiber, for 4-QAM and for a E_b/N_o of 5 dB; b) Transmitted constellation diagram for 35 meters of fiber, for 4-QAM and for a E_b/N_o of 5 dB.

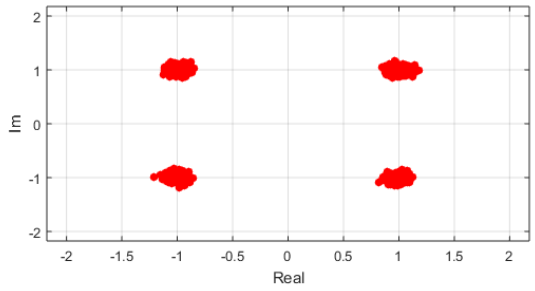

Figure 3.3 - Received constellation diagram for 35 meters of fiber, for 4-QAM and for a E_b/N_o of 5 dB.

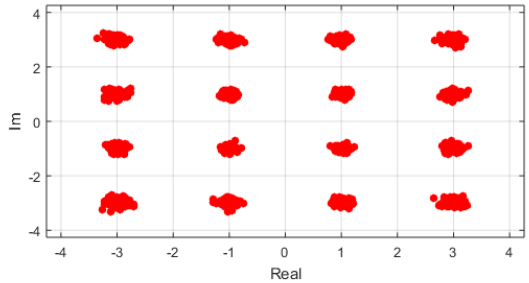

Figure 3.4 - Received constellation diagram for 35 meters of fiber, for 16-QAM and for a E_b/N_o of 5 dB.

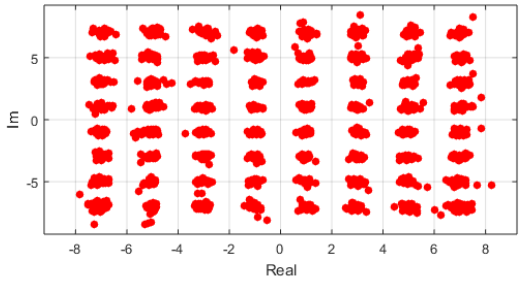

Figure 3.5 - Received constellation diagram for 35 meters of fiber, for 16-QAM and for a E_b/N_o of 5 dB.

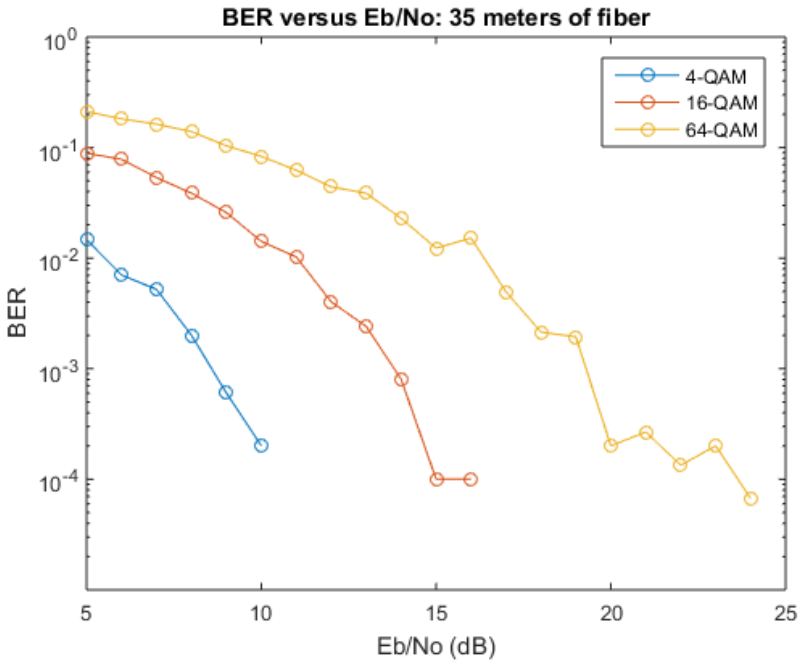

Figure 3.6 – Diagram of the obtained BER versus E_b/N_o for 4-QAM (blue), 16-QAM (red) and 64-QAM (yellow), for 35 meters of fiber.

From Figure 3.7 to Figure 3.9 there are presented the received constellation diagram of the received signal for 4-QAM, 16-QAM and 64-QAM, simulating the transmission over 100 meters of fiber, created with *Matlab*. Figure 3.10 shows the diagram of the obtained BER versus E_b/N_o for 4-QAM, 16-QAM and 64-QAM, for 100 meters of fiber.

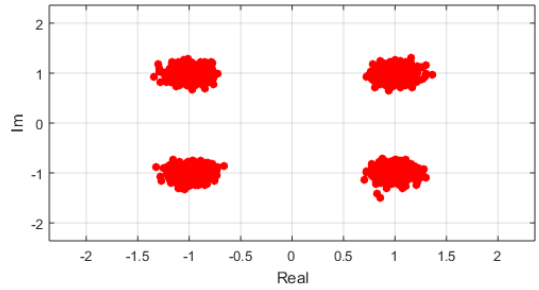

Figure 3.7 - Received constellation diagram for 100 meters of fiber, for 4-QAM and for a E_b/N_o of 5 dB.

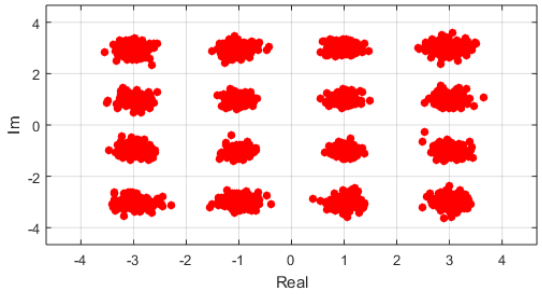

Figure 3.8 - Received constellation diagram for 100 meters of fiber, for 16-QAM and for a E_b/N_o of 5 dB.

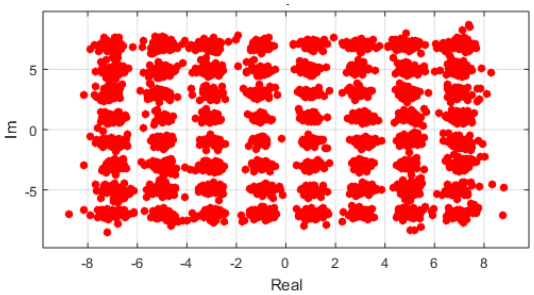

Figure 3.9 - Received constellation diagram for 100 meters of fiber, for 64-QAM and for a E_b/N_o of 5 dB.

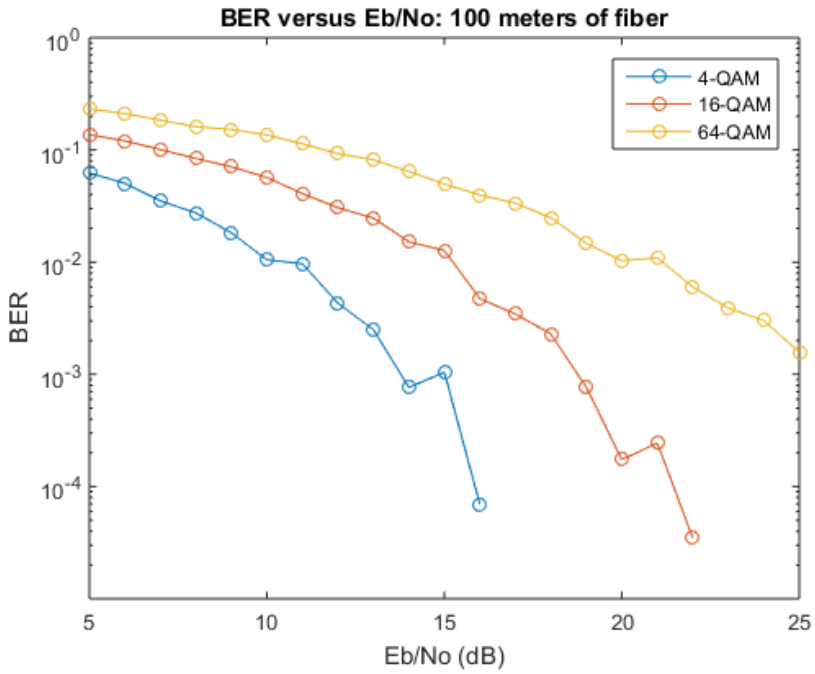

Figure 3.10 - Diagram of the obtained BER versus E_b/N_o for 4-QAM (blue), 16-QAM (red) and 64-QAM (yellow), for 100 meters of fiber.

Comparing the simulation results presented above, with 35 meters of fiber the BER is lower than with 100 meters of fiber because the dispersion in the fiber is also lower. One can also note that for higher levels of QAM modulation the BER is lower because each symbol carries less energy and the symbols are closer to each other in the constellation, increasing the probability of obtaining an error bit. Likewise, with the increase of the fiber distance and in the QAM modulation level there is an increase in the transmission rate, which increases the SNR, which can be explained by equation (3.3).

4. Experimental Implementation

4.1. Objectives

The experimental setup was based on the block diagram of Figure 2.12. The transmission of the OFDM signal through the POF was divided in three blocks. The first one was to create the signal using a *Matlab* script according to the parameters chosen for this work (number of total and information subcarriers, available bandwidth, cyclic prefix duration and the level of QAM-mapping). In the second block, the signal was used to directly modulate the LED using a DAC and then it propagates in the POF, being converted to the electrical domain through a PIN photodiode. An ADC converts the received signal into a digital signal and, at the final part, the signal is demodulated also with *Matlab* and the evaluation parameters BER is calculated. For the transmitter three different LEDs were used: IF-E92B which has a blue optical signal, operating at 470 nm peak wavelength, IF-E93 which has a green optical signal, operating at 522 nm, and IF-E96E, which has a red optical signal, operating at 650 nm, all from *Industrial Fiber Optics*. For the receiver it was used the PIN photodiode IF-D91, also from *Industrial Fiber Optics*. The DAC and ADC used for the experiment was *Analog Discovery* from *Digilent*, and for the transmission channel there were used two different lengths of POF, 35 and 100 meters, HFBR-EUS100Z from *Broadcom Limited*. The POF used in this work displayed the characteristics mentioned in Table 1.

Attenuation	$0.22\ \mathrm{dB/m}$
Numerical Aperture (NA)	0.47
Core and Cladding diameter	$1\ \mathrm{mm}$
Core refractive index (n_{core})	1.492
Cladding refractive index ($n_{cladding}$)	1.417

Table 1 - HFBR-EUS100Z POF characteristics [61].

Observing the characteristics of the POF used in this work, one can determine its pulse broadening due to modal dispersion using equation (2.3), obtaining the following results:

$$\Delta t = \frac{L_1}{2c \times 1{,}417} \times 0{,}47^2 \Leftrightarrow \frac{\Delta t}{L_1} = 0{,}257\ \mathrm{ns/m} \tag{4.1}$$

As mentioned in subsection 2.2.1, the LED must operate in the quasi-linear segment of its characteristic, through DCO-OFDM. Therefore, the DC characteristics of the LEDs were measured with

the power supply PS613, from *Velleman*, and the multimeter 75-MY64, from *Vitecom*, to measure its forward current. In Figure 4.1 there are shown the characteristics of the three LEDs.

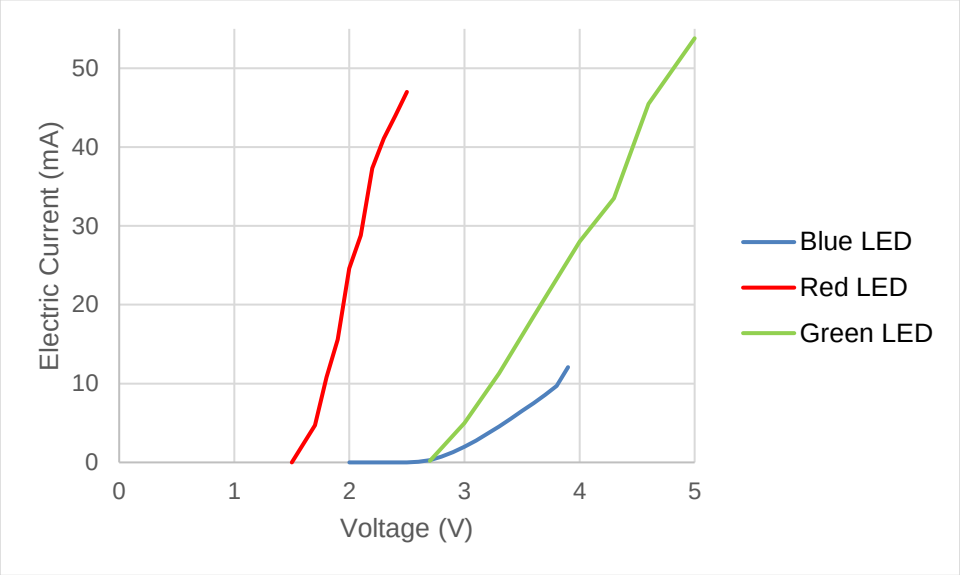

Figure 4.1 - LED's characteristic: electric current as a function of the applied voltage.

As it can be observed in the LEDs' characteristics presented, for the blue one the quasi-linear segment is from 3.0 V to 3.8 V, for the green one it is the segment from 3.0 V to 4.8 V and for the red one it is from 1.7 V to 2.5 V. However, for the green and red LEDs it occurred the saturation of the photodiode in this segment, so in this work it is used the segment from 3.0 V to 3.8 V and the segment from 1.7 V to 2.1 V for the green and red LED, respectively. The receiver setup used in this work was shown in Figure 2.7, and the input resistance chosen was 47 kHz, because it presented the best relationship between bandwidth and sensitivity.

To determine the bandwidth of the system a sinusoid signal generated using *Waveforms*, which is a software developed by *Digilent*, was injected into the LEDs and the amplitude of the output signal was measured for different frequencies, using the 35 and 100 meters of fiber length. The bandwidth is often defined by the frequency which the output signal is half-attenuated, also known as the cut-off frequency. Measuring the electrical amplitude of the output signal A at a certain frequency divided by the maximum amplitude of the signal A_o, the cut-off frequency is defined as the -3 dB frequency. This method to determine an electrical system's bandwidth with multimode fibers is simple and reliable to estimate the transmission capacity without performing very complicated experiments [62]. Figure 4.2 and Figure 4.3 show the obtained system's response for the 35 and 100 meters length of fiber, respectively, for the green LED, as an example.

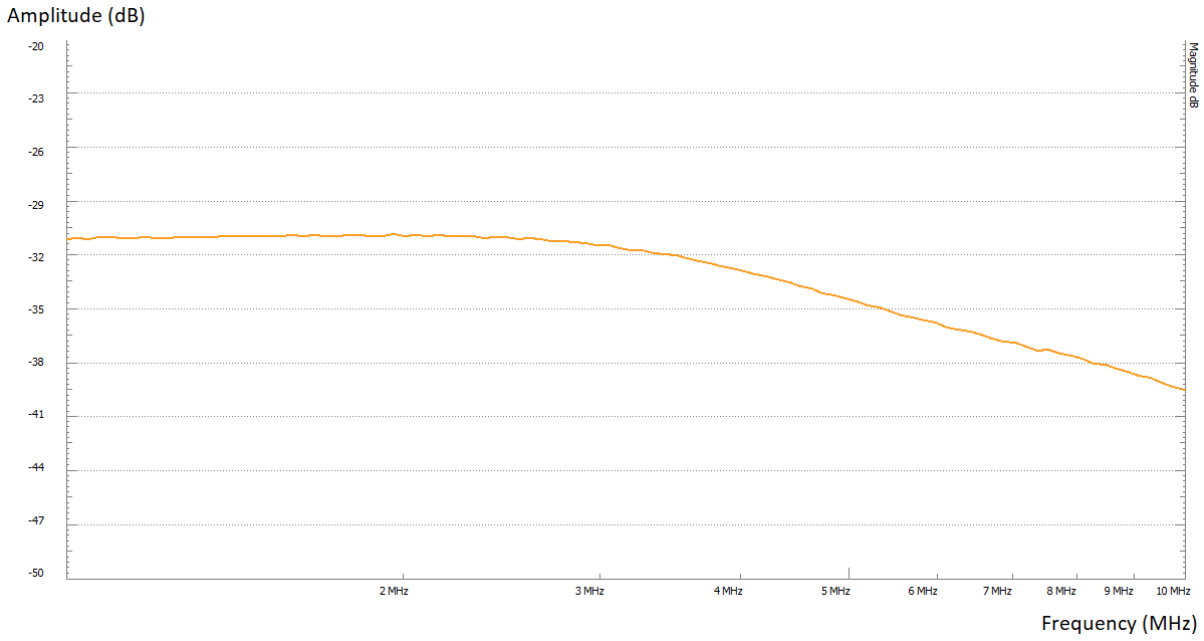

Figure 4.2 - System's response for the green LED for 35 meters of fiber: the amplitude A/A_o in dB as function of the signal's frequency. It shows that its $-3\mathrm{dB}$ bandwidth is about $4.8\ \mathrm{MHz}$.

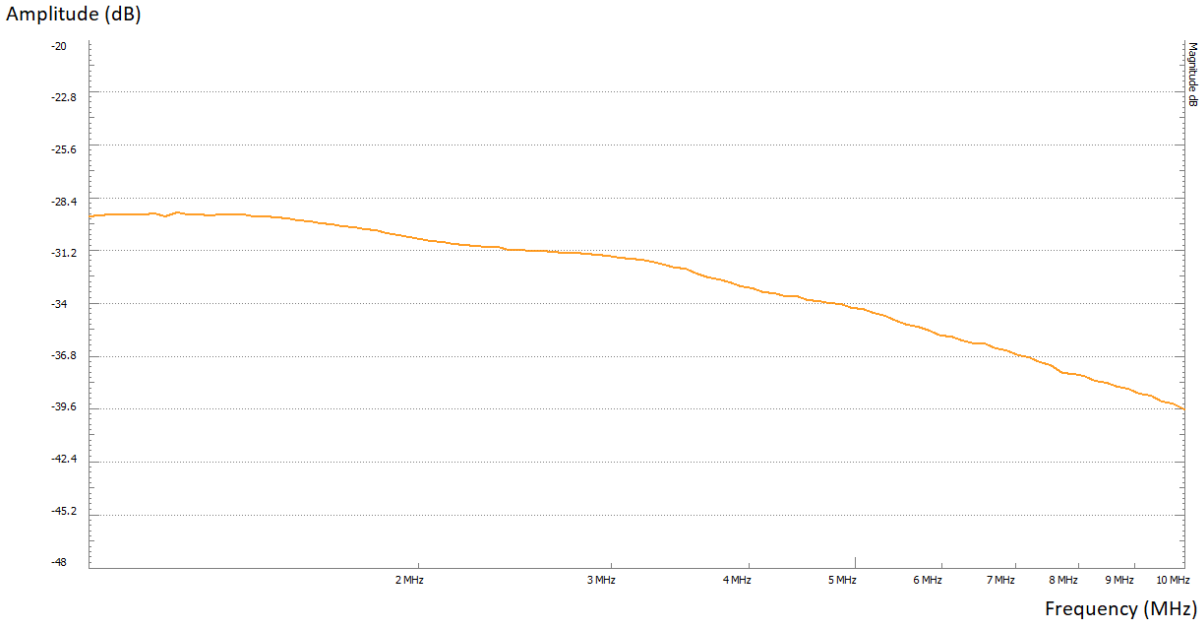

Figure 4.3 - System's response for the green LED for 100 meters of fiber: the amplitude A/A_o in dB as function of the signal's frequency. It shows that its $-3\mathrm{dB}$ bandwidth is about $4.4\ \mathrm{MHz}$.

One of the reasons why the amplitude of the signal is decreasing with the frequency is that the optical power generated by the LED decreases as the frequency increases, because the current variations are not as fast as the electron/hole recombination in the semiconductors.

The determined bandwidths for the three LEDs and for the 35 and 100 meters of fiber are presented in Table 2.

	35 m	100 m
Green LED	4.8 MHz	4.4 MHz
Blue LED	4.6 MHz	4 MHz
Red LED	5.7 MHz	4.1 MHz

Table 2 - 3dB system's bandwidth.

One can observe that the system's bandwidth for the 100 meters of fiber is lower than for the 35 meters systems, and it can be expected by the expression relating the fiber length of a POF with the available bandwidth, described in equation (2.4).

Figure 4.4 shows the photograph of the implemented system with 100 meters of fiber.

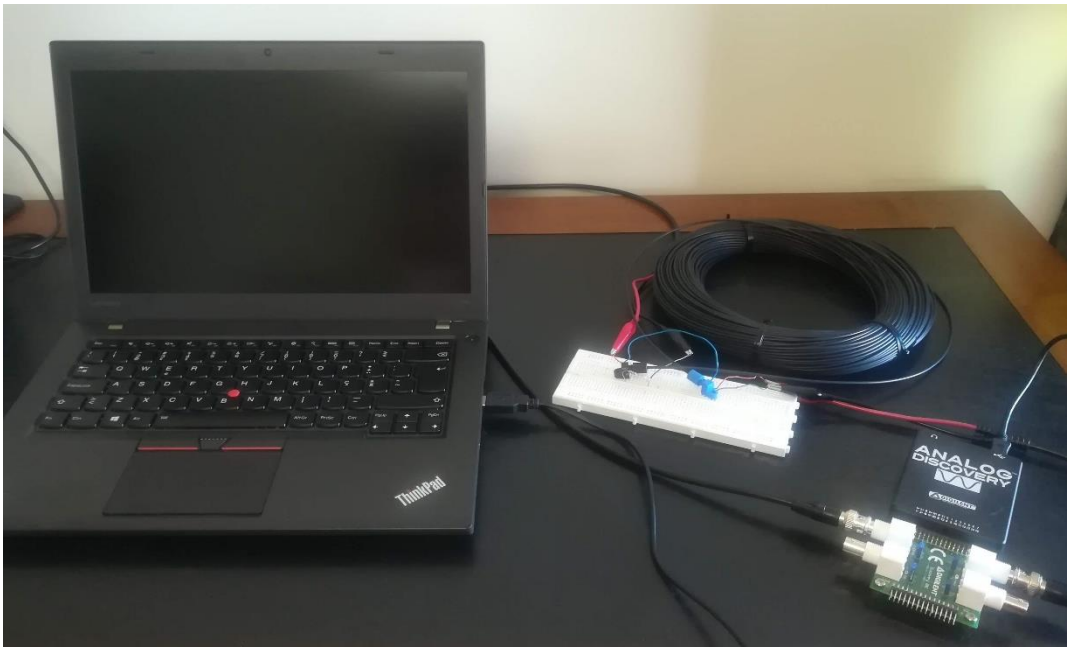

Figure 4.4 - Implemented system with 100 meters of fiber.

4.2. Parameters for the OFDM system

As mentioned in subsection 2.1.1, modal dispersion occurs when using optical fibers. The duration of the cyclic prefix has a relationship between the impulsive channel response to prevent ICI. Hence, the duration of the cyclic prefix usually is 2 to 4 times the modal delay, i.e., $2\Delta t \leq T_g \leq 4\Delta t$. The useful

duration of the OFDM symbol is 5 to 10 times the modal delay, which means, $5\Delta t \leq T_u \leq 10\Delta t$. Composed by subcarriers separated by $\Delta f = 1/T_u$, the total duration of the OFDM symbol can be expressed as:

$$T_s = T_u + T_g \tag{4.2}$$

The number of data subcarriers, before Hermitian Symmetry is applied, can therefore be obtained as:

$$N_{HS} = \frac{B}{\Delta f} = B.T_u \tag{4.3}$$

The number of total subcarriers needs to be a power of two to decrease the complexity of the FFT algorithm, and in order to have that a zero padding is added in the middle of the IFFT block to maintain the Hermitian Symmetry and for the spectrum to be centered in the available frequency interval.

Because the modal dispersion is very low in this work, to decrease the frequency spacing between subcarriers, a factor of 100 was used in the modal delay to determine the duration of the cyclic prefix. Hence, the parameters of the OFDM system for the two fiber lengths are represented in Table 3. It was assumed a total bandwidth B of 12 MHz for calculating the parameters, in order to have a higher number of subcarriers, because the modal dispersion is very low.

Parameters	35 m fiber	100 m fiber
Δt	$0.91\ \mu s$	$2.57\ \mu s$
T_g	$2\Delta t = 1.82\ \mu s$	$2\Delta t = 5.14\ \mu s$
T_u	$10\Delta t = 9.10\ \mu s$	$10\Delta t = 25.67\ \mu s$
T_s	$10.92\ \mu s$	$30.81\ \mu s$
Δf	110 kHz	38.97 kHz
N_{HS}	110	308
N_{IFFT}	256	512
N_{sc}	$\frac{N_{HS}}{2} - 1 = 54$	$\frac{N_{HS}}{2} - 1 = 153$

Table 3 - Projected parameters for the OFDM system.

For the parameters described, different levels of QAM-mapping were used: 4-QAM, 16-QAM and 64-QAM. The sampling frequency of the DAC and ADC must be, accordingly to the Nyquist Theorem, at least two times the available bandwidth:

$$f_{sampling} \geq 2B \tag{4.4}$$

Thus, the sampling frequency was chosen to be 100 MHz. After the first part is performed in *Matlab*, as shown in Figure 4.5, the signal is sent to the DAC, travels through the different lengths of optical fiber, and then the demodulation process starts, as it can be described in Figure 4.6.

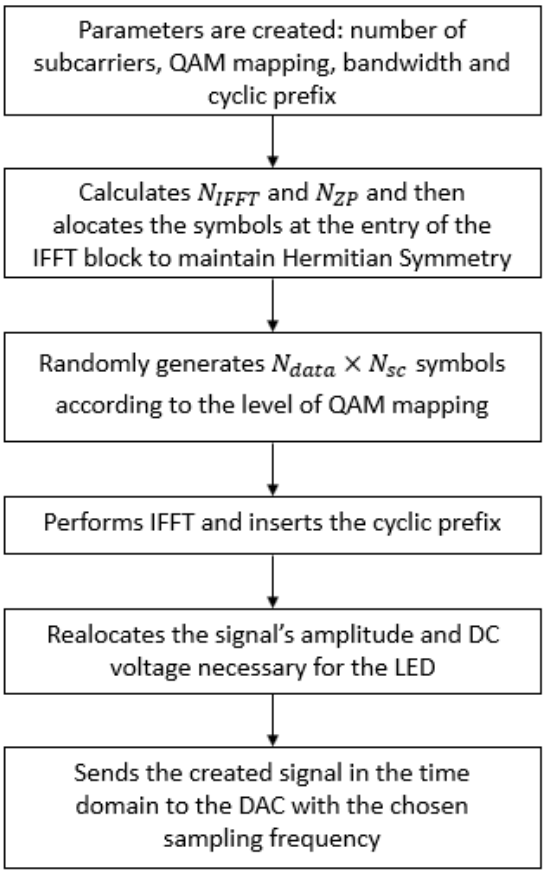

Figure 4.5 - Diagram of the modulation process in *Matlab*.

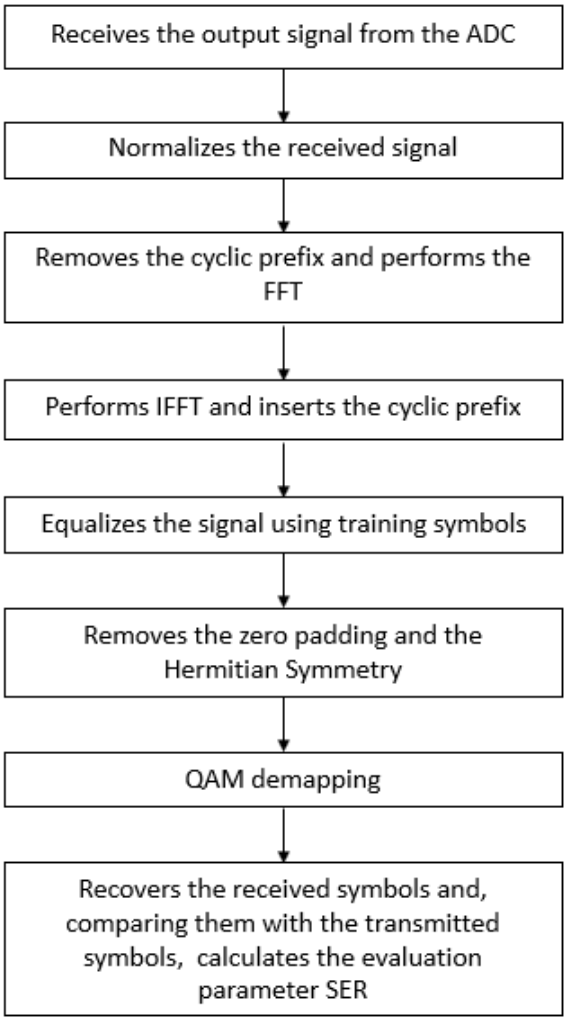

Figure 4.6 - Diagram of the demodulation process in *Matlab*.

Note that in real systems, the receptor does not know the transmitted signal, so there could not be a performance evaluation of the transmission.

5. Results and Analysis

The results obtained in the experiment described in the previous chapter are now presented and analyzed. The transmissions performed in this work involved three different scenarios. The first one was to measure the optical back-to-back with a piece of fiber with length of approximately 6 cm to make sure that the amplitude chosen for the signal would not saturate neither the LED nor the photodiode. The other two were the transmission over 35 and 100 meters of fiber for the three different LEDs. Also, in order to study the impact of the equalizer for having a robust system, two different training symbols lengths were tested for the 35 meters length.

5.1. Transmission over 35 meters of fiber

2700 samples were transmitted over 35 meters of fiber, with a simulation time of $10.92\ \mu s$ and 256 total subcarriers were used. With 2700 samples transmitted and 162 of them used for the equalizer (6%), for 4-QAM, 16-QAM and 64-QAM, the total number of bits sent was 5394, 10788 and 21576, respectively. From Figure 5.1 to Figure 5.4 there are represented the transmitted OFDM signal and transmitted QAM constellation, and the QAM constellation of the received signal, for an equalization of 6% and for the blue LED, over 35 meters of fiber. The results were obtained with the *Matlab* script as detailed in section 4. Figure 5.2, Figure 5.3 and Figure 5.4 were obtained through the analyses of the demodulated signal.

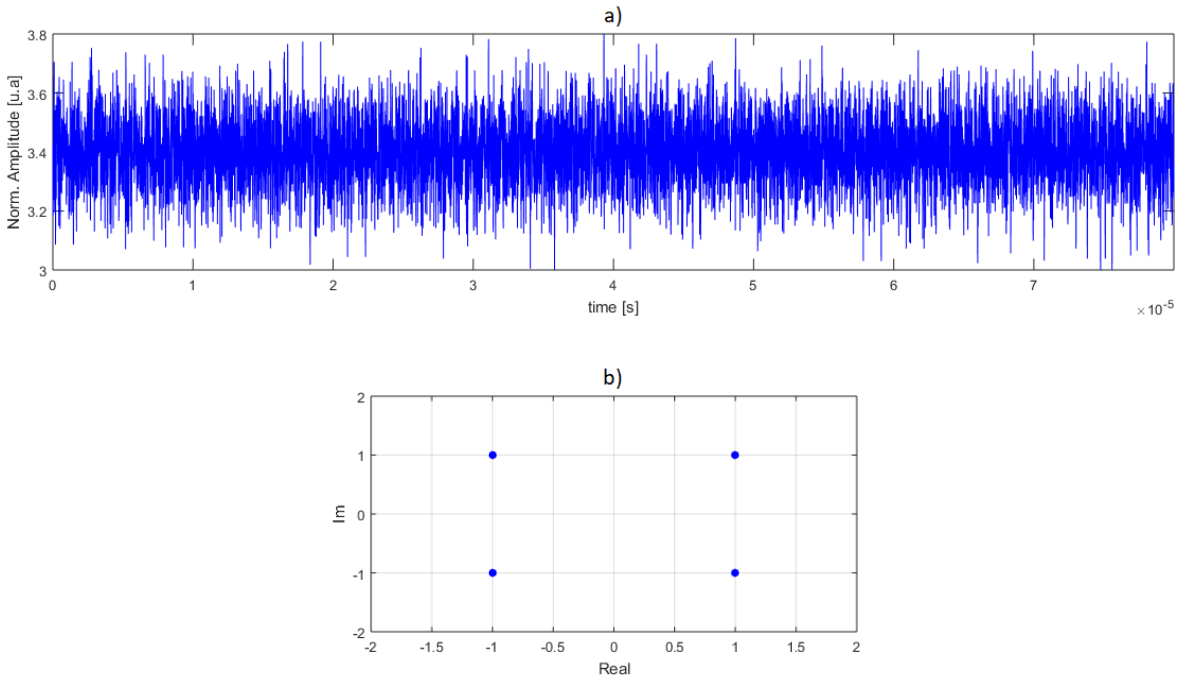

Figure 5.1 – a) Transmitted OFDM symbol in the time domain for 4-QAM, 35 meters of fiber and for the blue LED; b) QAM constellation diagram of the transmitted signal for 4-QAM, 35 meters of fiber and for the blue LED.

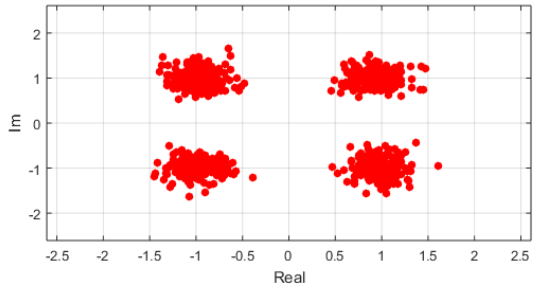

Figure 5.2 – QAM constellation diagram of the received signal for 4-QAM and 35 meters of fiber, for a received optical power of $-16.92\ \mathrm{dBm}$.

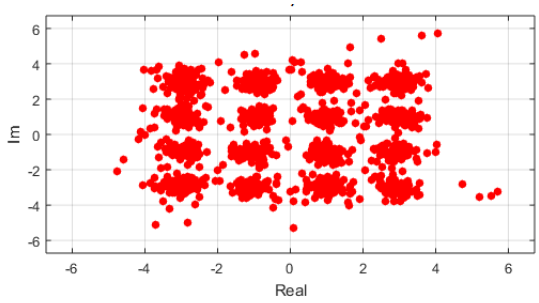

Figure 5.3 - QAM constellation diagram of the received signal for 16-QAM and 35 meters of fiber, for a received optical power of $-17.30\ \mathrm{dBm}$.

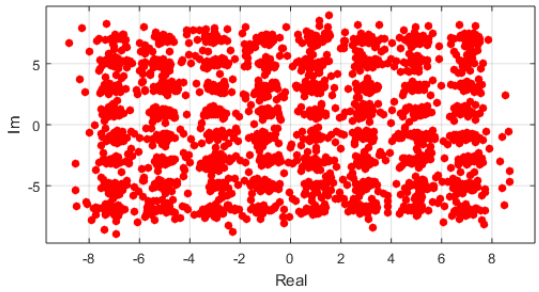

Figure 5.4 - QAM constellation diagram of the received signal for 16-QAM and 35 meters of fiber, for a received optical power of $-17.33\ \mathrm{dBm}$.

Comparing the constellation diagrams of the received signal between 4-QAM, 16-QAM and 64-QAM one can see that for higher modulation levels the closer the QAM symbols are, increasing the probability or error. The constellations are not rotated, however the symbols are horizontally dislocated, which is an effect of the fiber dispersion. The noise in the received constellation diagrams is higher for higher QAM modulation levels, as it was expected.

To test if better results would be accomplished with more training symbols, they were increased to 20% of the total symbols, and the results are presented in Figure 5.5.

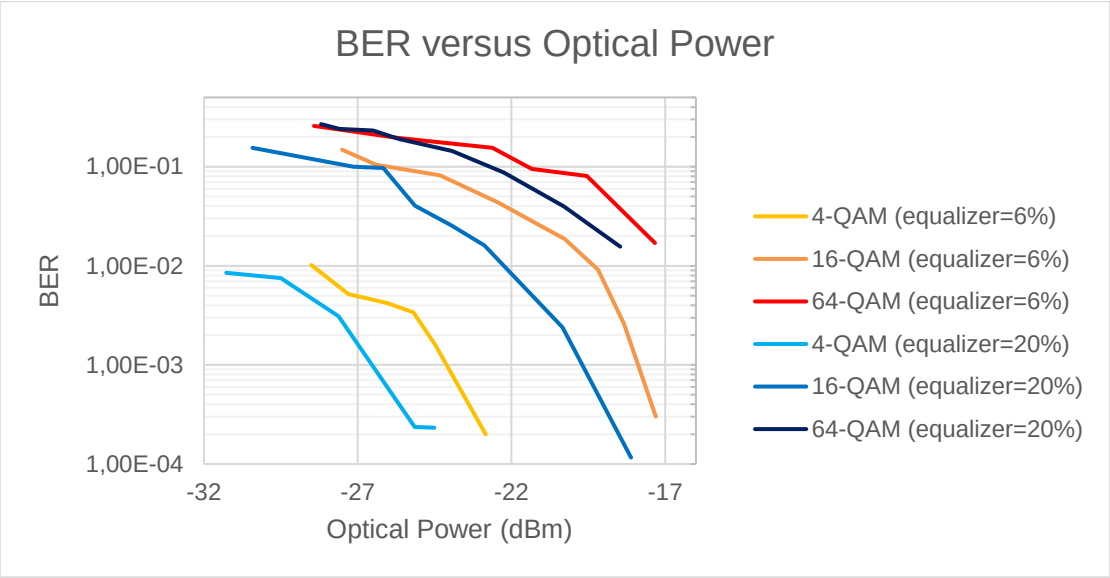

Figure 5.5 – BER versus optical power at the receiver, for the two training symbol lengths and for 4-QAM, 16-QAM and 64-QAM, for the blue LED.

The optical power measured at the receiver was determined with equation (2.13). The photodiode's responsivity $\mathcal{R}$ is $0.4\ \mathrm{A/W}$. Knowing the tension in the input resistance terminals and its value, the current I_{ph} can be determined and then the optical power P_{opt} is measured.

With more training symbols the BER obtained for the same optical power is lower for every QAM modulation than with less training symbols, with the cost of having a lower transmission rate and spectral efficiency. All the transmissions reported could be achieved with FEC, because the obtained BER were below the FEC limit.

The best results achieved with the transmission over 35 meters of fiber were a BER of 2.0×10^{-4} for 4-QAM, with the three LEDs, a BER of 1.0×10^{-4} for 16-QAM and with the red LED, and a BER of 5.5×10^{-4} for 64-QAM and also with the red LED. For some of the obtained results zero erroneous bits were reported, which means that only one error in $(N_{data} - N_t)N_{sc}\log_2 M$ total bits could be detected, obtaining the measured BER. The curves of the obtained BER versus the optical power at the receiver for each LED are presented in Figure 5.6, Figure 5.7 and Figure 5.8, for each level of QAM modulation.

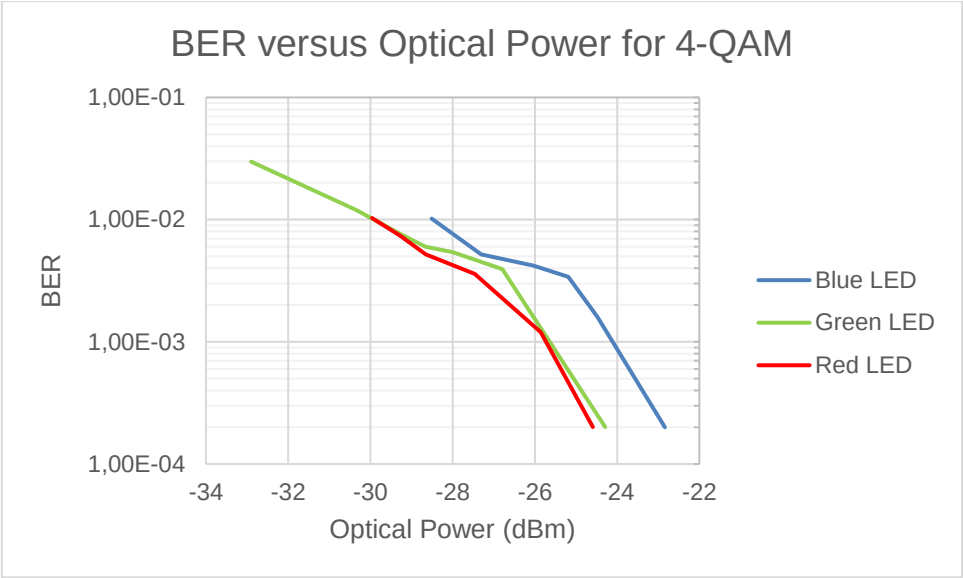

Figure 5.6 - BER versus optical power at the receiver for 4-QAM, for 35 meters of fiber.

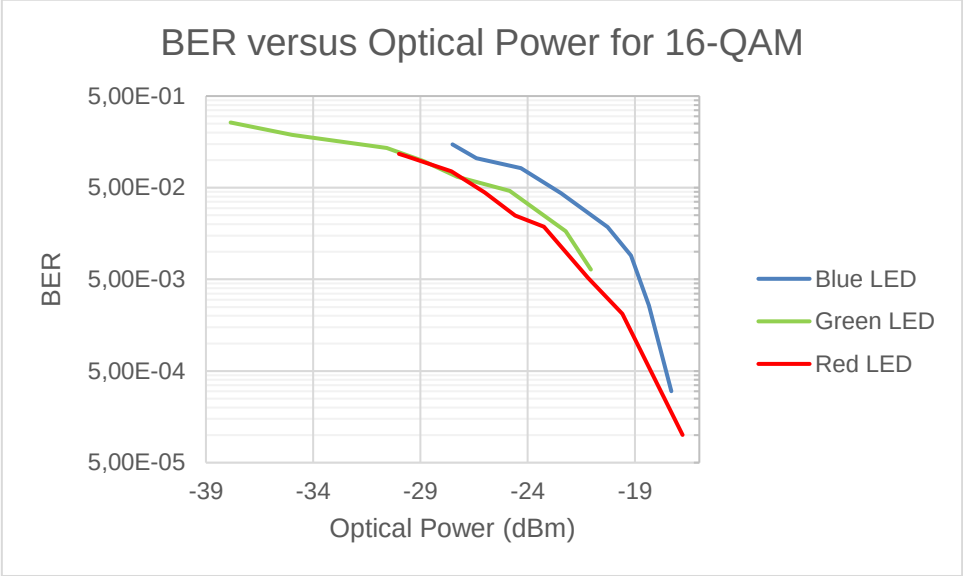

Figure 5.7 - BER versus optical power at the receiver for 16-QAM, for 35 meters of fiber.

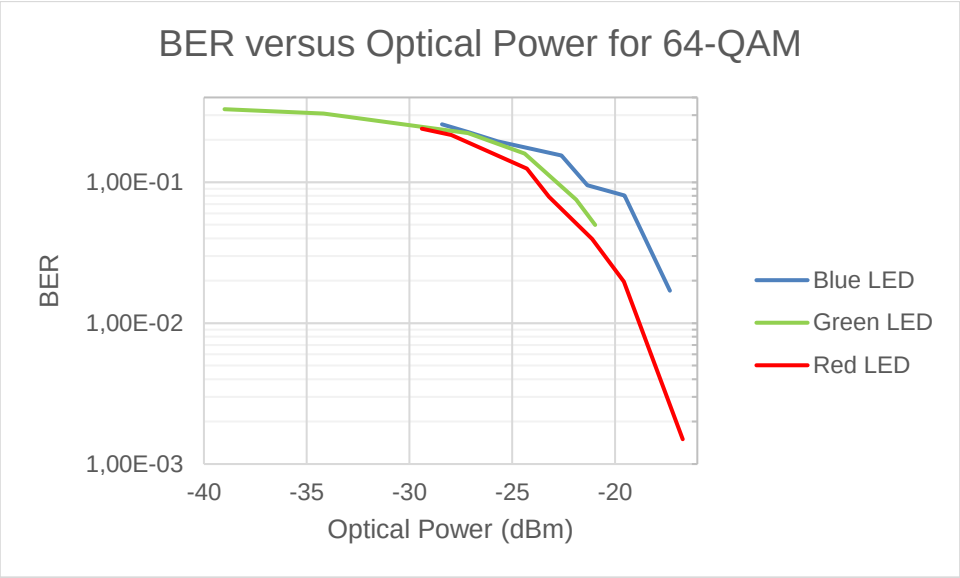

Figure 5.8 - BER versus optical power at the receiver for 64-QAM, for 35 meters of fiber.

The blue LED shows to have the highest BER at the same optical power, and this results are expected as the system with the blue LED presents the lowest available bandwidth. Figure 5.9 and Figure 5.10 show the lowest obtained BER and spectral efficiency, respectively, for the three LEDs and for different QAM level modulations.

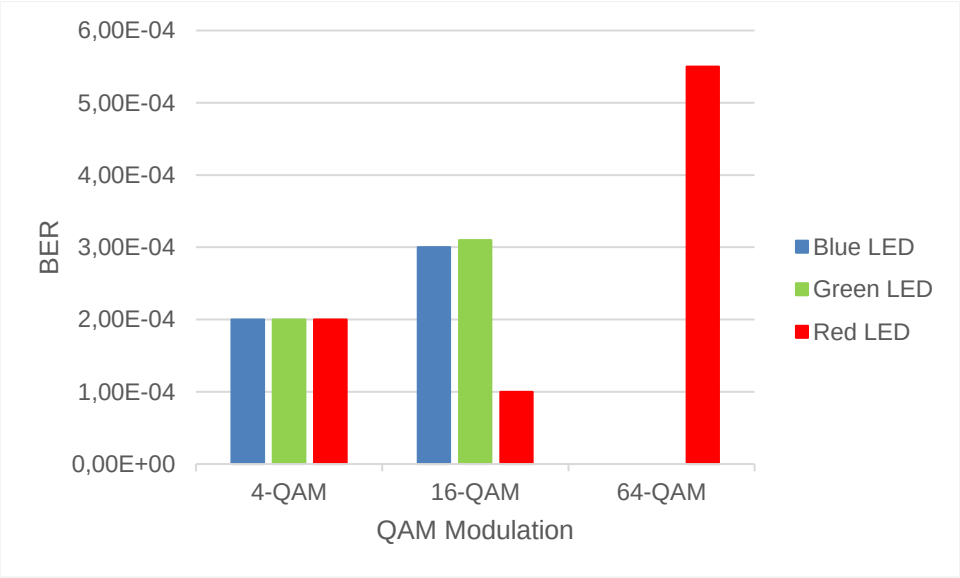

Figure 5.9 - Obtained BER for the three LEDs and for 4-QAM and 16-QAM for 35 meters of fiber.

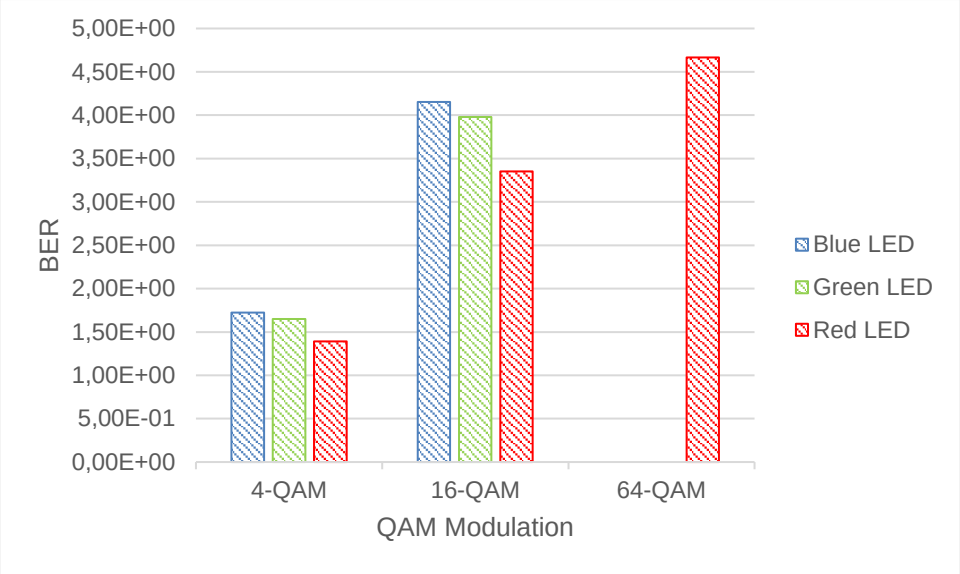

Figure 5.10 - Obtained spectral efficiency S for the three LEDs and for 4-QAM and 16-QAM for 35 meters of fiber.

5.2. Transmission over 100 meters of fiber

7650 samples were transmitted with a simulation time of $30.81\ \mu s$ and 512 total subcarriers were used. With 7650 samples transmitted and 459 of them used for the equalizer (6%), for 4-QAM, 16-QAM and 64-QAM, the total number of bits sent was 15294, 30588 and 61176, respectively. From Figure 5.11 to Figure 5.13 there are represented the transmitted OFDM signal and QAM constellation, and the QAM constellation of the received signal, for an equalization of 6% and for the blue LED, over 100 meters of fiber. The results were obtained with the *Matlab* script as detailed in section 4. Figure 5.12 and Figure 5.13 were obtained through the analyses of the demodulated signal.

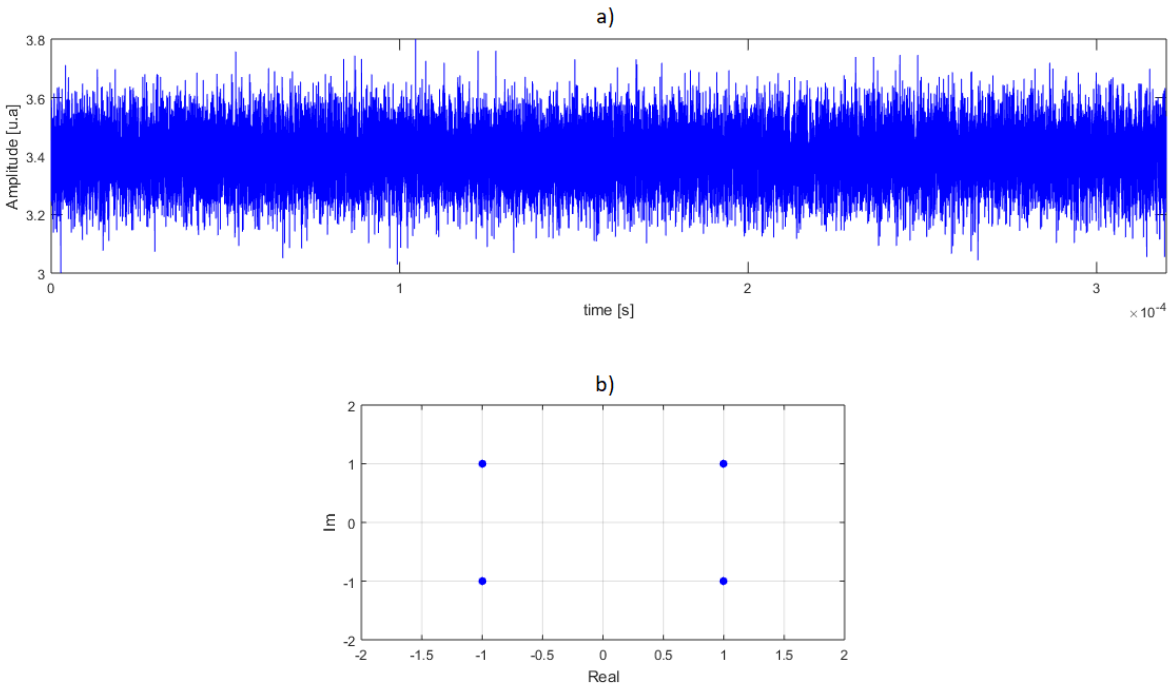

Figure 5.11 - a) Transmitted OFDM symbol in the time domain for 4-QAM, 100 meters of fiber and for the blue LED; b) QAM constellation diagram of the transmitted signal for 4-QAM, 100 meters of fiber and for the blue LED.

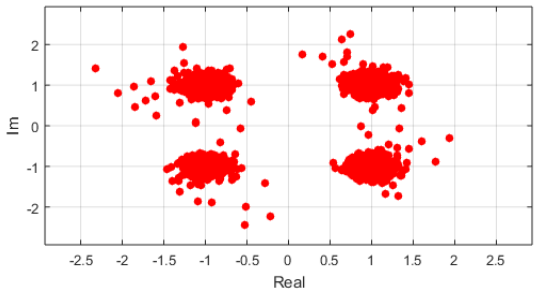

Figure 5.12 - QAM constellation diagram of the received signal for 4-QAM and 100 meters of fiber, for a received optical power of $-20.17\ \mathrm{dBm}$.

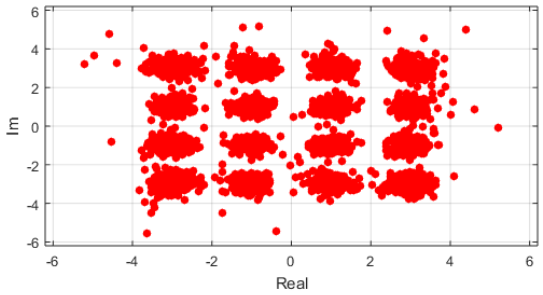

Figure 5.13 - QAM constellation diagram of the received signal for 16-QAM and 100 meters of fiber, for a received optical power of $-20.12\ \mathrm{dBm}$.

Comparing the constellation diagrams of the received signal between 4-QAM and 16-QAM it can also be seen that for higher modulation levels the closer the QAM symbols are, increasing the probability of error, and the constellations are also not rotated. The noise in the received constellation diagrams is not higher than for 35 meters of fiber. The curves of the obtained BER versus the optical power at the receiver for each LED are presented in Figure 5.14, Figure 5.15 and Figure 5.16, for each level of QAM modulation and for the transmission over 100 meters of fiber.

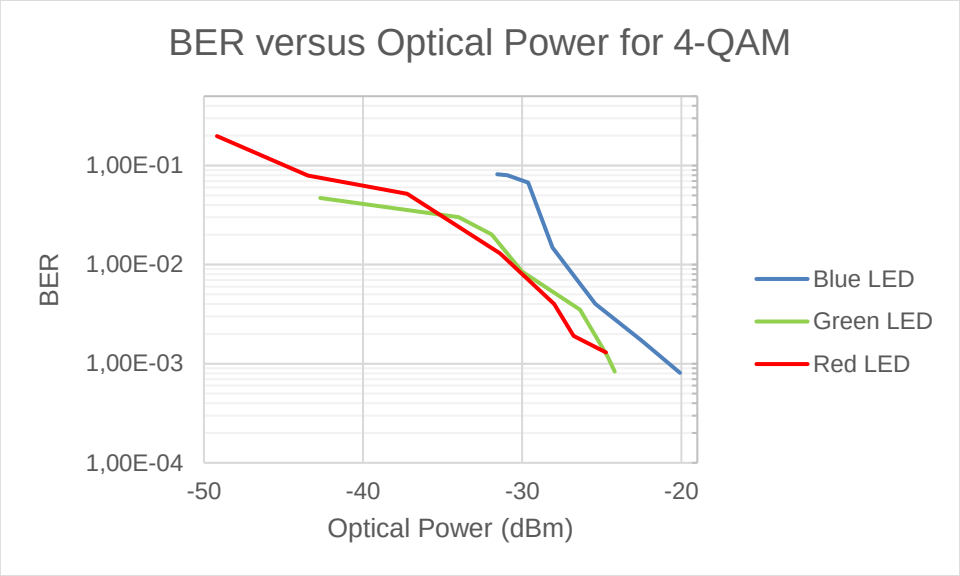

Figure 5.14 - BER versus optical power at the receiver for 4-QAM, for 100 meters of fiber.

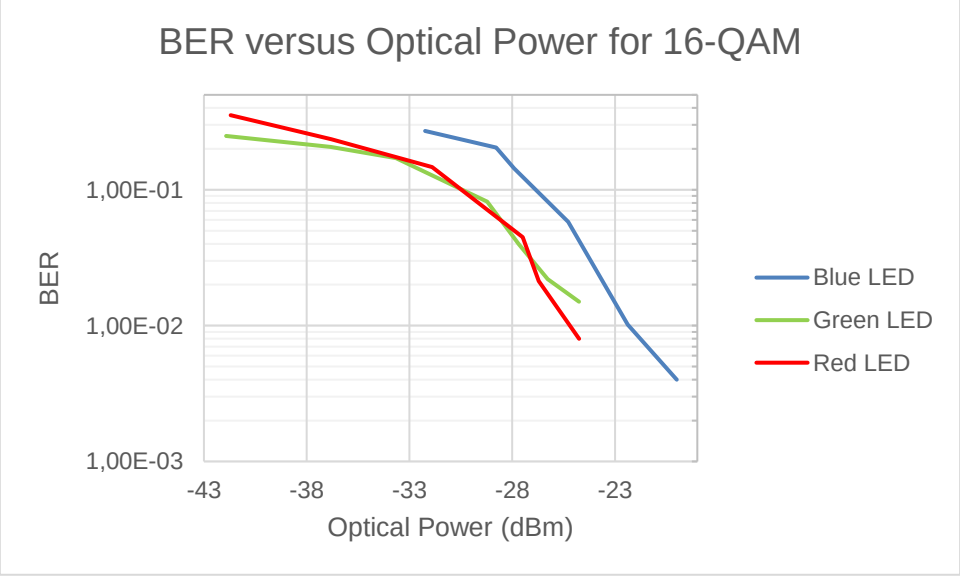

Figure 5.15 - BER versus optical power at the receiver for 16-QAM, for 100 meters of fiber.

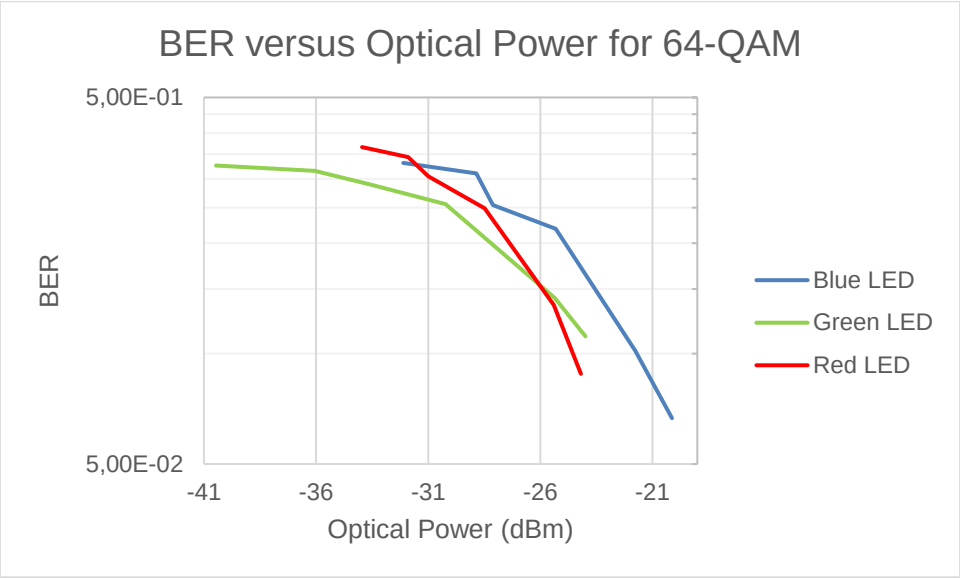

Figure 5.16 - BER versus optical power at the receiver for 64-QAM, for 100 meters of fiber.

The green and red LED shows to have the lowest BER for the same optical power, and the blue LED shows to have the highest BER, as it presents the lowest available bandwidth. Figure 5.17 and Figure 5.18 show the obtained BER and spectral efficiency, respectively, for the three LEDs and for different QAM level modulations, for 100 meters of fiber.

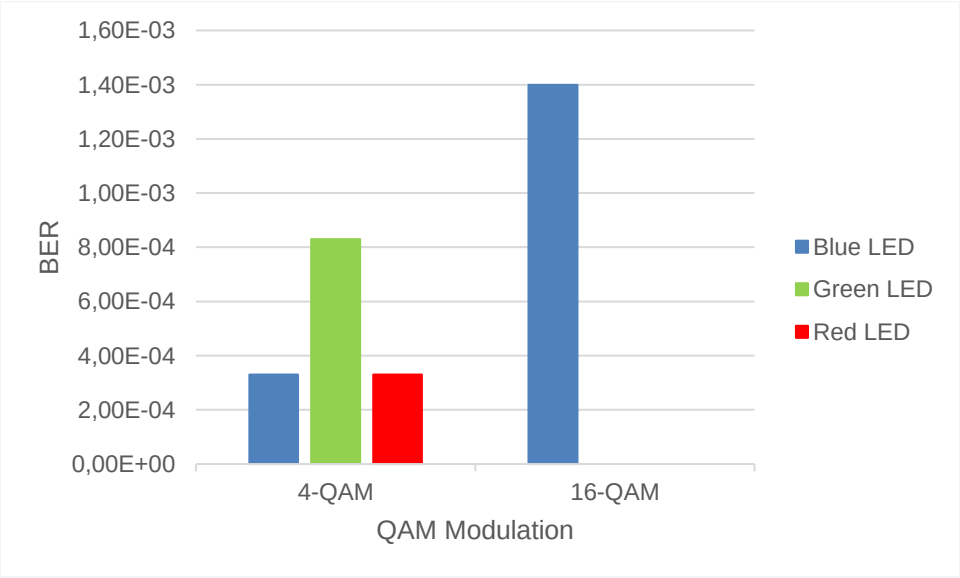

Figure 5.17 – Obtained BER for the three LEDs and for 4-QAM and 16-QAM for 100 meters of fiber.

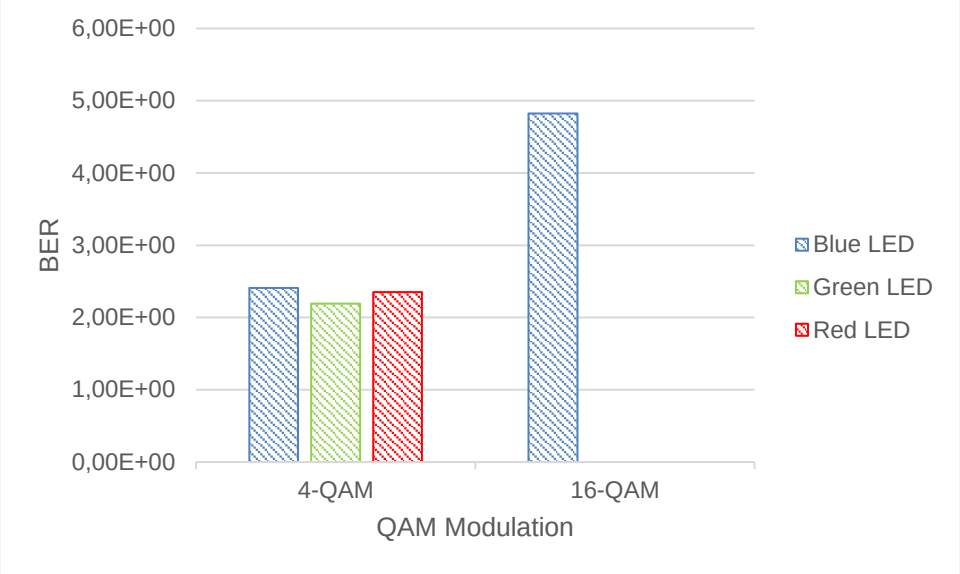

Figure 5.18 - Obtained spectral efficiency S for the three LEDs and for 4-QAM and 16-QAM for 100 meters of fiber.

5.3. Comments on results

Comparing the transmission over 35 and 100 meters of fiber it can be observed that the red LED suffers from attenuation the most, because for the 35 meters transmission the optical power at the receiver with the green and blue LED was higher, and for 100 meters transmission the optical power with the red LED reduced to the same optical power as obtained with the green LED. This fact can be confirmed with Figure 2.2, which indicates that the red optical signal suffers more attenuation through the fiber that green or blue optical signal. For the 35 meters transmission, the transmission rate record for the blue LED was $19.1\ \mathrm{Mb/s}$, with a spectral efficiency of $4.15\ \mathrm{b/s/Hz}$, and the same transmission rate was achieved by the green LED, with a spectral efficiency of $3.98\ \mathrm{b/s/Hz}$. For the red LED a transmission rate of $26.6\ \mathrm{Mb/s}$ with a spectral efficiency of $4.67\ \mathrm{b/s/Hz}$ was accomplished. For the 100 meters transmission, a transmission rate of $9.64\ \mathrm{Mb/s}$ with the green and red LED, with a spectral efficiency of $2.19\ \mathrm{b/s/Hz}$ and $2.35\ \mathrm{b/s/Hz}$, respectively, and a transmission rate of $19.3\ \mathrm{Mb/s}$ with the blue LED, with a spectral efficiency of $4.83\ \mathrm{b/s/Hz}$, were achieved.

6. Conclusions

This final chapter intends to summarize the results and main conclusions of this work as well as to propose some topics to develop in the future. The suggested topics are related not only to some improvements that can be made but also additional goals that enrich and look forward to an engineering project regarding optical communications.

6.1. Summary

OFDM is a well-known modulation technique in wireless systems and appears as an interesting approach in optical communication systems in access and long-distance networks. The major advantages of using OFDM is its efficiently way of using multiple subcarriers to overcome the effects of dispersion in a transmission channel, namely optical fibers: the orthogonality between subcarriers allows them to spectrally overlap, optimizing the occupied bandwidth, and the insertion of a guard interval is essential to cancel the effects of the channel dispersion, which could lead to ISI. Moreover, the IFFT/FFT algorithm has a low complexity, and therefore the costs of the system are reduced. The optical OFDM signal is, unlike the wireless OFDM, is a baseband and purely real signal, thanks to the Hermitian symmetry, but with the cost of a lower transmission rate.

In the transmissions performed, OFDM signals were generated with *Matlab* and then sent to a DAC. The applied offset and peak-to-peak voltage are chosen so that the LEDs and photodiode operate in their linear regimes. The OFDM signal directly modulates the LED and the ADC captures the received signal, at the receiver, and the *Matlab* demodulates it. The obtained results show that the transmissions do suffer from the effects of the fiber dispersion, because the constellations of the received symbols with 35 and 100 meters of fiber were horizontally deslocated, and they suffer from noise and attenuation, due to the LEDs and photodiode, respectively, and the fiber itself. Transmissions of $26.6\ \mathrm{Mb/s}$ over 35 meters of fiber and $19.3\ \mathrm{Mb/s}$ over 100 meters of fiber with LEDs emitting on wavelengths corresponding to blue, red and green in the visible spectrum and with the non-coherent detection of a PIN photodetector were accomplished. The goal of overcoming the effects of the fiber dispersion was achieved and the transmissions' spectral efficiency has reached $7.19\ \mathrm{b/s/Hz}$ with the red LED and over the 35 meters transmission. Despite the transmissions were successful, there is a lot of work that can be done in order to improve their performance.

6.2. Future work

The OFDM system performance can be significantly improved by dynamically adapting the transmission parameters, such as power, constellation size, symbol rate, and coding rate/scheme, according to the channel conditions. The resilience to the channel conditions can be further enhanced if information about the channel is sent over a return-channel. Based on this feedback information, adaptive modulation (AMO-OFDM), channel coding and power allocation may be applied across all subcarriers, or individually to each subcarrier. To improve the system's BER, adaptive bit allocation can

be employed such that the information is redistributed across the subcarriers, according to the channel state information (bit-loading algorithm). The optimization process steps can be simplified as:

1. A maximum BER is established. A high-level mapping is sent, for example 256-QAM, and if the BER of one subcarrier is greater than the established BER, a lower level of mapping is applied in that subcarrier, for example 128-QAM: otherwise, the applied mapping level remains. The same process is repeated until all the subcarriers' BER follows the imposed limit.
2. As soon as all of the subcarriers have an adequate mapping scheme, the OFDM frames can be sent according to the acquired information in the first step.

Some bit-loading algorithms were proposed by Chow, Cioffi and Bingham [63], Liu and Tang proposed a power-loading algorithm with uniform bit-loading that aimed to minimize the transmit power while guaranteeing a target BER [64]. Leke and Cioffi proposed a finite granularity algorithm that maximized the data rate for a given margin: subcarriers with SNR below a predefined threshold were nulled, then the remaining subcarriers were identified, and the available power was distributed either optimally using a water-filling approach or sub-optimally by assuming equal power to maximize the data rate [65]. In [66], the authors proposed a non-iterative low complexity optimal allocation algorithm that mutually maximizes the throughput and minimizes the transmit power, while guaranteeing a target BER per subcarrier. Besides the bit-loading and power-loading algorithms, codification schemes (COFDM) can be used in the symbols to protect the transmitted information.

7. References

[1] Cisco, "The Zettabyte Era: Trends and Analysis," 2017.

[2] W. Daum, J. Krauser, P. E. Zamzow and O. Ziemann, POF - Polymer Optical Fibers for Data Communication, New York: Springer, 2002.

[3] H. Murofushi, "Low loss perfluorinated POF," in *Fifth International Conference on Plastic Optical Fibres and Applications - POF'96*, Paris, 1996.

[4] X. Wang, "OFDM and its Application to 4G," in *4th Annual Wireless and Optical Communications Conference*, 2005.

[5] Y. Koike and M. Asai, "The future of plastic optical fiber," *Asia Materials,* vol. 1, pp. 22-28, 2009.

[6] Y. Koike, "POF from the Past to the Future," in *Proceedings of the 7th International Conference of Plastic Optical Fibre*, Berlin, 1998.

[7] Y. Koike, "High Bandwidth and Low Loss Polymer Optical Fiber," in *Proceedings of the 1st International Conference on Plastic Optical Fibres and Applications*, Paris, 1992.

[8] S. Loquai, R. Kruglov, O. Ziemann, J. Vinogradov and C. Bunge, "10 Gbit/s over 25 m plastic optical fiber as a way for extremely low-cost optical interconnection," in *OFC/NFOEC*, 2010.

[9] R. W. Chang, "High-Speed Multichannel Data Transmission with Bandlimited Orthogonal Signals," *Bell System Tech. J.,* vol. 45, pp. 1775-1796, December 1966.

[10] B. R. Saltzberg, "Performance of an Efficient Parallel Data Transmission System," *IEEE Transactions on Communication Technology,* vol. 6, pp. 805-811, Dec 1967.

[11] S. B. Weinstein and P. M. Ebert, "Data Transmission by Frequency-Division Multiplexing Using the Discrete Fourier Transform," *IEEE Transactions on Communication Technology,* vol. 5, pp. 628-634, October 1971.

[12] A. Peled and A. Ruiz, "Frequency Domain Data Transmission Using Reduced Computational Complexity Algorithms," *IEEE,* vol. III, pp. 964-967, 1980.

[13] L. J. Cimini, "Analysis and Simulation of a Digital Mobile Channel," *IEEE Transactions on Communications,* vol. 33, pp. 665-675, July 1985.

[14] M. Alard and R. Lassalle, "Principles of Modulation and Channel Coding for Digital Broadcasting for Mobile Receivers," *EBU Technical Review,* vol. 224, pp. 168-190, 1987.

[15] J. S. Chow, J. C. Tu and J. M. Cioffi, "A Discrete Multitone Transceiver System for HDSL Applications," *IEEE Journal on Selected Areas in Communications,* vol. 9, pp. 895-908, 1991.

[16] U. Reimers, "Digital Video Broadcasting," *IEEE Communications Magazine,* vol. 36, pp. 104-110, 1998.

[17] Y. Li, J. H. Winters and N. R. Sollenberg, "MIMO-OFDM for Wireless Communications: Signal Detection With Enhanced Channel Estimation," *IEEE Transactions on Communications,* vol. 50, pp. 1471-1477, September 2002.

[18] S. H. Han and J. H. Lee, "An Overview of Peak-to-Average Power Ratio Reduction Techniques for Multicarrier Transmission," *IEEE Wireless Communications,* vol. 12, pp. 56-65, April 2005.

[19] C. Pradabpet, K. Eupree, S. Chivapreecha and K. Dejhan, "A New PAPR Reduction Technique for OFDM-WLAN in 802.11a Systems," in *Ninth ACIS International Conference on Software Engineering, Artificial Intelligence, Networking, and Parallel/Distributed Computing*, 2008.

[20] T. R. Rao and A. Giulietti, "A Performance Study on the 802.11g WLAN OFDM System," in *The International Conference on Computer as a Tool*, 2005.

[21] P. Xiao, C. Toal, D. Burns and V. Fusco, "Transmit and Receive Filter Design For OFDM based WLAN systems," in *International Conference on Wireless Communications and Signal Processing*, 2010.

[22] I. Koffman and V. Roman, "Broadband Wireless Access Solutions Based on OFDM Access in IEEE 802.16," *IEEE Communications Magazine,* vol. 40, pp. 96-103, 2002.

[23] G. Dong, H. Chen, M. Yang and J. Dai, "Dynamic Frequency Selection (DFS) in IEEE8O2.16e OFDM System Working at Unlicensed Bands," in *The 9th International Conference on Advanced Communication Technology*, 2007.

[24] Y. Jin, Z. Zheng, . X. Wang and Y. Zhang, "IEEE802.16e DOA Estimation Technology over MIMO-OFDM Channel," in *International Joint Conference on Computational Sciences and Optimization*, China, 2009.

[25] A. N. Akansu and X. Lin, "A Comparative Performance Evaluation of DMT (OFDM) and DWMT (DSBMT) based DSL Communications Systems for Single and Multitone Interference," in *IEEE International Conference on Acoustics, Speech and Signal Processing*, 1998.

[26] P. Falcone, F. Colone, C. Bongioanni and P. Lombardo, "Experimental Results for OFDM WiFi-based Passive Bistatic Radar," in *IEEE Radar Conference*, 2010.

[27] J. Anatory, N. Theethayi and R. Thottappillil, "Effects of Multipath on OFDM Systems for Indoor Broadband Power-Line Communication Networks," *IEEE Transactions on Power Delivery,* vol. 24, pp. 1190-1197, July 2009.

[28] W. Roh, J. Y. Seol, J. H. Park, B. H. Lee, J. K. Lee, J. S. Kim, J. Cho, K. W. Cheun and F. Aryanfar, "Milimeter-Wave Beamforming as an Enabling Technology for 5G Cellular Communications: Theoretical Feasibility and Prototype Results," *IEEE Communications Magazine,* vol. 52, pp. 106-113, 2014.

[29] S. Chen and J. Zhao, "The requirements, challenges, and technologies for 5G of terrestrial mobile communication," *IEEE Communications Magazine,* vol. 52, pp. 36-43, May 2014.

[30] O. Gonzalez, R. Perez-Jimenez and S. Rodriguez, "Adaptive OFDM System for Communications Over the Indoor Wireless Optical Channel," *IEE Proceedings - Optoelectronics,* vol. 153, pp. 139-144, 2006.

[31] J. Grubor, V. Jungnickel and K.-D. Langer, "Adaptive Optical Wireless OFDM System with Controlled Asymmetric Clipping," in *Conference Record of the Forty-First Asilomar Conference on Signals, Systems and Computers*, USA, 2007.

[32] R. Mesleh, H. Elgala and H. Haas, "On the Performance of Different OFDM Based Optical Wireless Communication Systems," *IEEE Journal of Optical Communications and Networking,* vol. 3, pp. 620-628, 2011.

[33] B. J. C. Schmidt, A. J. Lowery and J. Armstrong, "Experimental Demonstrations of Electronic Dispersion Compensation for Long-Haul Transmission Using Direct-Detection Optical OFDM," *Journal of Lightwave Technology,* vol. 26, pp. 196-203, 2008.

[34] W. Shieh and C. Athaudage, "Coherent Optical Orthogonal Frequency Division Multiplexing," *Electronics Letters,* vol. 42, pp. 587-589, 2006.

[35] S. L. Jansen, I. Morita, T. C. W. Schenk, N. Takeda and H. Tanaka, "Coherent Optical 25.8-Gb/s OFDM Transmission," *Journal of Lightwave Technology,* vol. 26, pp. 6-15, 2008.

[36] J. M. Tang and K. A. Shore, "Maximizing the Transmission Performance of Adaptively Modulated Optical OFDM Signals in Multimode-Fiber Links by Optimizing Analog-to-Digital Converters," *Journal of Lightwave Technology,* vol. 25, pp. 787-798, 2007.

[37] J. M. Tang, P. M. Lane and K. A. Shore, "Transmission Performance of Adaptively Modulated Optical OFDM Signals in Multimode Fiber Links," *IEEE Photonics Technology Letters,* vol. 18, pp. 205-207, 2006.

[38] A. J. Lowery and J. Armstrong, "10 Gbit/s Multimode Fiber Link Using Power-Efficient Orthogonal-Frequency-Division Multiplexing," *Optics Express,* vol. 13, p. 10003–10009, 2005.

[39] S. C. J. Lee, F. Breyer, S. Randel, O. Ziemann, H. P. A. van den Boom and A. M. J. Koonen, "Low-Cost and Robust 1-Gbit/s Plastic Optical Fiber Link Based on Light-Emitting Diode Technology," in *Optical Fiber Communication/National Fiber Optic Engineers Conference*, USA, 2008.

[40] J. Silva , R. Ribeiro, A. Barbero and M. Segatto, "Optical Orthogonal Frequency Division Multiplexing through 20 m and 100 m Step-Index Polymer Optical Fibers Using Red, Green and Blue Light Emitting Diodes," 2010.

[41] I. B. Djordjevic, B. Vasic and M. Neifeld, "LDPC-Coded OFDM for Optical Communication Systems with Direct Detection," *IEEE Journal of Selected Topics in Quantum Electronics,* vol. 13, pp. 1446-1454, 2007.

[42] C. Chen, C. Zhang, D. Liu, K. Qiu and S. Liu, "Tunable optical frequency comb enabled scalable and cost-effective multiuser orthogonal," *Optics Letters,* vol. 37, pp. 3954-3956, 2012.

[43] C. Chen, C. Zhang, W. Zhang, W. Jin and K. Qiu, "Hybrid WDM-OFDMA-PON utilising tunable generation of flat optical comb," *Electronics Letters,* vol. 49, pp. 276-277, 2013.

[44] C. Chen, W. Zhong, X. Li and D. Wu, "MDPSK-based nonequalization OFDM for coherent free-space optical communication," *IEEE Photonics Technology Letters,* vol. 26, pp. 1617-1620, 2014.

[45] T. Komine and M. Nakagawa, "Fundamental Analysis for Visible-Light Communication System using LED Lights," *IEEE Transactions on Consumer Electronics,* vol. 50, pp. 100-107, February 2004.

[46] J. Armstrong and S. D. Dissanayake, "Comparison of ACO-OFDM, DCO-OFDM and ADO-OFDM in IM/DD Systems," *IEEE Journal of Lightwave Technology,* vol. 31, no. 7, pp. 1063-1072, April 2013.

[47] O. Ziemann, J. Krauser, P. E. Zamzow and W. Daum, POF Handbook: Optical Short Range Transmission Systems, Germany: Springer, 2008.

[48] G. P. Agrawal, Fiber-Optic Communication Systems, John Wiley & Sons, 2002.

[49] A. Bunge, "The Way to 1-Gbit/s POF Home Networks: The Work of the International Standardisation Group DKE 412.7.1," in *FTTH Conference 2011*, 2011.

[50] I. Stefan, H. Elgala, R. Mesleh, D. O'Brien and H. Haas, "Optical Wireless OFDM System on FPGA: Study of LED Nonlinearity Effects," in *IEEE 73rd Vehicular Technology Conference*, Japan, 2011.

[51] C.-A. Bunge, T. Gries and M. Beckers, Polymer Optical Fibers, Elsevier, 2017.

[52] ThorLabs, "Unmounted Photodiodes LAB Facts".

[53] N. Marchetti, M. I. Rahman, S. Kumar and R. Prasad, "OFDM: Principles and Challenges," in *New Directions in Wireless Communications Research*, V. Tarkh, Ed., Springer, 2009.

[54] W. C. Lee, Mobile Cellular Telecommunications Systems, New York, USA: McGraw-Hill, December, 1989.

[55] J. G. Proakis and M. Salehi, Digital Communications, 5th ed., McGraw-Hill, 2008.

[56] J. Armstrong, "OFDM for Optical Communications," *Journal of Lightwave Technology,* vol. 27, February 1, 2009.

[57] [Online]. Available: http://www.revolutionwifi.net/revolutionwifi/2015/3/how-ofdm-subcarriers-work.

[58] Z. Wu, "MIMO-OFDM Communication Systems: Channel Estimation and Wireless Location," Louisiana, 2006.

[59] S. O. Popescu, G. Budura and A. S. Gontean, "Review of PSK and QAM — Digital modulation techniques on FPGA," in *International Joint Conference on Computational Cybernetics and Technical Informatics*, Romania, 2010.

[60] F. Chang, K. Onohara and T. Mizuochi, "Forward error correction for 100 G transport networks," *IEEE Communications Magazine,* vol. 48, pp. S48-S55, 2010.

[61] B. Limited, *Plastic Optical Fiber Cable and Accessories,* HFBR-RXXYYYZ Data Sheet.

[62] X. Q. Jin and J. M. Tang, "Effectiveness of the Use of 3-dB Bandwidths of Multimode Fibres for Estimating the Transmission Performance of Adaptively Modulated Optical OFDM Signals Over IMDD Links," *Journal of Lightwave Technology,* vol. 27, no. 18, pp. 3992-3998, 2009.

[63] P. S. Chow, J. M. Cioffi and J. A. C. Bingham, "A practical discrete multitone transceiver loading algorithm for data transmission over spectrally shaped channels," *IEEE Transactions on Communications,* vol. 43, pp. 773-775, 1995.

[64] K. Liu, B. Tang and Y. Liu, "Adaptive power loading based on unequal-ber strategy for OFDM systems," *IEEE Communications Letters,* vol. 13, pp. 474-476, 2009.

[65] A. Leke and J. M. Cioffi, "A maximum rate loading algorithm for discrete multitone modulation systems," in *IEEE Global Telecommunications Conference*, USA, 1997.

[66] E. Bedeer, M. F. Marey, O. A. Dobre, M. H. Ahmed and K. E. Baddour, "A novel algorithm for joint bit and power loading for OFDM systems with unknown interference," in *IEEE International Conference on Communications*, Canada, 2012.